Cellulose-Synthesizing Machinery in Bacteria

Kenji Tajima (ktajima@eng.hokudai.ac.jp)
Hokkaido University https://orcid.org/0000-0002-3238-813X
Tomoya Imai
Kyoto University
Toshifumi Yui
University of Miyazaki
Min Yao
Hokkaido University
Inder Saxena
The University of Texas at Austin

Research Article

Keywords: bacterial cellulose (BC), terminal complex (TC), cellulose synthase, cellulose, synthesizing mechanism, bcs operon, Gluconacetobacter

Posted Date: June 22nd, 2021

DOI: https://doi.org/10.21203/rs.3.rs-633140/v1

Version of Record: A version of this preprint was published at Cellulose on October 1st, 2021. See the published version at https://doi.org/10.1007/s10570-021-04225-7.

Cellulose-synthesizing machinery in bacteria

Kenji Tajima,[1,*] Tomoya Imai,[2] Toshifumi Yui,[3] Min Yao,[4] and Inder Saxena,[5,*]

[1]*Faculty of Engineering, Hokkaido University, N13W8, Kita-ku, Sapporo 060-8628, Japan*

[2]*Research Institute for Sustainable Humanosphere, Kyoto University, Gokasyo, Uji-shi, Kyoto 611-0011, Japan*

[3]*Faculty of Engineering, University of Miyazaki, Gakuen-kibanadai- nishi-1-1, Miyazaki 889-2192, Japan*

[4]*Faculty of Advanced Life Science, Hokkaido University, N10W8, Kita-ku, Sapporo 060-0810, Japan*

[5]*Department of Molecular Biosciences, The University of Texas at Austin, Austin, TX 78712, USA*

*Corresponding author

e-mail address: ktajima@eng.hokudai.ac.jp

e-mail address: imsaxena@austin.utexas.edu

ORCID number

Kenji Tajima: 0000-0002-3238-813X
Tomoya Imai: 0000-0001-7026-0287
Toshifumi Yui: 0000-0002-6939-7750
Min Yao: 0000-0003-1687-5904
Inder Saxena: 0000-0003-1952-8676

Keywords: *bacterial cellulose (BC); terminal complex (TC); cellulose synthase; cellulose; synthesizing mechanism; bcs operon; Gluconacetobacter*

Abstract

Cellulose is produced by all plants and a number of other organisms, including bacteria. The most representative cellulose-producing bacterial species is *Gluconacetobacter xylinus* (*G. xylinus*), an acetic acid bacterium. Cellulose produced by *G. xylinus*, commonly referred to as bacterial cellulose (BC), has exceptional physicochemical properties resulting in its use in a variety of applications. All cellulose-producing organisms that synthesize cellulose microfibrils have membrane-localized protein complexes (also called terminal complexes or TCs) that contain the enzyme cellulose synthase and other proteins. The bacterium *G. xylinus* is a prolific cellulose producer and a model organism for studies on cellulose biosynthesis. The widths of cellulose fibers produced by *Gluconacetobacter* are 50–100 nm, suggesting that cellulose-synthesizing complexes are nanomachines spinning a nanofiber. At least four different proteins (BcsA, BcsB, BcsC, and BcsD) are included in TC from *Gluconacetobacter*, and the proposed function of each is as follows: BcsA, synthesis of a glucan chain through glycosyl transfer from UDP-glucose; BcsB, complexes with BcsA for cellulose synthase activity; BcsC, formation of a pore in the outer membrane through which a glucan chain is extruded; BcsD, regulates aggregation of glucan chains through four tunnel-like structures. In this review, we discuss structures and functions of these four and a few other proteins that have a role in cellulose biosynthesis in bacteria.

Introduction

Cellulose, an assembly of b-1,4-linked linear glucan chains, is the most abundant polysaccharide and biopolymer. It is used widely, without and with further modifications (such as ether and ester derivatives), in a number of industries including clothing, pulp and paper, food, pharmaceuticals, cosmetics, and building materials. Most cellulose is synthesized as a major component of the cell walls in plants, and it is estimated that between 10^{10} and 10^{11} tons of cellulose is produced each year (Hon 1994). Cellulose is an environmentally friendly and circulating polymer, as plants use carbon dioxide from the atmosphere during photosynthesis to produce the raw materials for cellulose biosynthesis, and it is broken down by a number of organisms.

In addition to plants, other organisms, including bacteria, produce cellulose as an extracellular polysaccharide. Cellulose biosynthesis is reported in a number of bacterial and cyanobacterial species (Napoli et al. 1975; Matthysse et al. 1981; Nobles et al. 2001; Otsuka et al. 2004; Kumagai et al. 2011; Kawano et al. 2011; Castro et al. 2013; Thongsomboon et al. 2018), but it is in the acetic acid bacteria where production of cellulose is best observed and studied. Even among the acetic acid bacteria, it is *Gluconacetobacter xylinus/Gluconacetobacter hansenii* (referred to as *Acetobacter xylinum* in earlier publications, and more recently classified in the genus *Komagataeibacter*) (Yamada and Yukphan 2008; Yamada et al. 2012) that have been studied extensively for cellulose biosynthesis, and where maximal amount of cellulose production is observed. Both these species of *Gluconacetobacter* are Gram-negative, rod-shaped, obligate aerobes that are widely used for bacterial cellulose production, and are the representative cellulose-producing bacterial species. Herein, we will refer to both these species as *G. xylinus*.

Cellulose synthesis in all organisms is catalyzed by the enzyme cellulose synthase, a transmembrane protein, that uses UDP-glucose as the substrate. In bacteria, cellulose synthase

is part of a cellulose-synthesizing machinery that most likely includes other proteins. A linear array of particles associated with cellulose synthesis was observed in *G. xylinus* by freeze-fracture electron microscopy (Brown et al. 1976), with each particle representing a large transmembrane protein complex and the site of cellulose synthesis. That other proteins, in addition to cellulose synthase, may be part of this complex is suggested by the identification of the gene for cellulose synthase as part of an operon in *G. xylinus* (Saxena et al. 1990; Wong et al. 1990; Saxena et al., 1994; Nakai et al. 1998; Umeda et al. 1999; Kawano et al. 2002b) and other bacteria (Römling and Galperin 2015), and by protein-localization studies (Kimura et al. 2001; Sunagawa et al. 2013; Sun et al. 2017).

The principal cellulose synthesis operons (*bcs* operons) in *G. xylinus* species contain 4 genes (*bcsA*, *bcsB*, *bcsC* and *bcsD*) or 3 genes (*bcsAB*, *bcsC* and *bcsD*) depending on the strain of *G. xylinus*. These genes (and proteins) have been also referred to as *cesA*/*acsA* (CeSA/AcsA), *cesB*/*acsB* (CeSB/AcsB), *cesAB*/*acsAB* (CeSAB/AcsAB), *cesC*/*acsC* (CeSC/AcsC) and *cesD*/*acsD* (CeSD/AcsD), but from now on it is preferable to use the *bcs* symbol for genes in the bacterial cellulose synthesis operon, and Bcs symbol for proteins coded by genes in the *bcs* operon.

Although cellulose synthase is the main component of the cellulose-synthesizing complex, other proteins have a role in cellulose synthesis in vivo. What are these other proteins, what role do they play in cellulose biosynthesis, and how do they interact with each other in the cellulose-synthesizing complex? Some information related to these questions is coming from structural studies, and in this review, we discuss structures of a few proteins, specifically those that are known to have a role in cellulose synthesis in *Gluconacetobacter* species. Even as the structure and role of individual proteins in cellulose biosynthesis is being worked out, the objective in most cases is to determine the structure of the complete cellulose-synthesizing complex that performs all the events in cellulose synthesis, starting with the

addition of glucose from UDP-glucose to a growing glucan chain (polymerization) to extrusion of glucan chains across the cell envelope.

Purified cellulose synthase from *G. xylinus* contained two polypeptides (BcsA and BcsB) (Lin and Brown, Jr. 1989), and BcsA was shown to bind to UDP-Glucose, and therefore, it was identified as the cellulose synthase catalytic subunit (Lin et al. 1990). Following identification of the cellulose synthesis operon (*bcs* operon) in *G. xylinus* (Wong et al. 1990; Saxena et al. 1994), other proteins that have a role in cellulose synthesis were identified. From analysis of mutants, it was shown that while BcsC is absolutely required for native cellulose synthesis, BcsD is not absolutely required (Saxena et al. 1994). Genetic and biochemical studies demonstrated that even as synthesis of cellulose (cellulose II to be more specific) could be carried out in vitro by just BcsA and BcsB, other protein(s) were required for synthesis of native cellulose (cellulose I) in vivo. The role of other proteins, in addition to those coded for by genes in the *bcs* operon, in native cellulose synthesis was suggested through analysis of mutants affected in cellulose production in *G. xylinus*. Interestingly, though not surprisingly, the genes for these proteins are present adjacent (both upstream and downstream) to the *bcs* operon in *G. xylinus* (Standal et al. 1994; Tonouchi et al. 1997; Nakai et al. 1998; Umeda et al. 1999; Tajima et al. 2001; Kawano et al. 2002b). Upstream of the *bcs* operon are two genes - one encoding endo-β-1,4-glucanase (CMCax) and the other encoding the cellulose complementing protein (Ccp) (Standal et al. 1994); downstream of the *bcs* operon is a gene encoding β-glucosidase (Bgl) (Tonouchi et al. 1997; Tajima et al. 2001; Kawano et al. 2002b). CMCax exhibits cellulose hydrolyzing activity (Standal et al. 1994; Kawano et al. 2002a; Yasutake et al. 2006) and its expression is induced at a later stage of growth (Kawano et al. 2008). Gene expression analyses of *bgl* and *cmcax* using real-time qRT-PCR suggest that increase in *cmcax* expression after 5 d cultivation is caused by an increase in gentiobiose (a β-1,6-linked disaccharide of D-glucose), possibly synthesized in a reaction catalyzed by Bgl. Earlier work showed that CMCax affects cellulose production in *G.*

122 *xylinus* (Tonouchi et al. 1995; Hyun Min et al. 1998; Kawano et al. 2002a); CMCax may play
123 a role in the regulation of cellulose synthesis together with Bgl (Kawano et al. 2008). The
124 function of Ccp in cellulose biosynthesis is not understood, but it is a protein that exists only
125 in some cellulose-synthesizing bacteria such as *Gluconacetobacter*. Since Ccp interacts with
126 BcsD, it is speculated that it plays a role in cellulose synthesis in collaboration with BcsD
127 (Sunagawa et al. 2013).

128 The first report of structure determination of a protein coded for by a gene in the *bcs*
129 operon of *G. xylinus* was that of BcsD (Hu et al. 2010). Since then, structures are obtained of
130 protein complexes from other organisms capable of in vitro cellulose synthesis, namely the
131 BcsA-BcsB complex from *Rhodobacter sphaeroides* (Morgan et al. 2013), and the
132 BcsABEFRQ (Abidi et al. 2021) and BcsABEFGRQ complexes (Acheson et al. 2021) from
133 *Escherichia coli*. Crystal structures have been obtained of the N-terminal part, containing the
134 TPR-domain, of BcsC from *Enterobacter* sp. CJF-002 (Nojima et al. 2017), and the C-
135 terminal pore-containing domain of BcsC from *E. coli* (Acheson et al. 2019). In addition,
136 structures of BcsZ from *E. coli* (Mazur and Zimmer 2011) and CMCax from *G. xylinus*
137 (Yasutake et al. 2006) are known. Given the possible function(s) of some of these proteins
138 and their known structures in a few cellulose-producing organisms, the emerging picture is
139 that the cellulose-synthesizing machinery in bacteria may be much more diverse than
140 originally thought of.

141 Although *G. xylinus* is the major cellulose-producing bacterium in nature, only a few
142 proteins with a role in cellulose biosynthesis from this bacterium have been characterized
143 structurally. At the same time, a wealth of information at the microscopic level is available on
144 cellulose biosynthesis in this bacterium. One of our objectives is to understand the protein
145 components at the sites of cellulose synthesis in *G. xylinus,* and how they may be associated
146 and regulated to produce ribbons of cellulose.
147

An overview of cellulose synthesis in bacteria

Since the first report of cellulose synthesis in bacteria (Brown 1886), the list of bacteria where cellulose production has been demonstrated, and the number of bacteria where genes for cellulose biosynthesis have been identified, has grown longer. In addition to the acetic acid bacteria that includes species of *Gluconacetobacter*, production of cellulose is demonstrated in bacterial species such as *Agrobacterium tumefaciens* (Matthysse et al. 1981), *E. coli* (Thongsomboon et al. 2018), *Rhizobium* (Napoli et al. 1975), *Enterobacter* (Otsuka et al. 2004) and others. Interestingly, analysis of genome sequences of a large number of bacteria led to identification of genes for cellulose biosynthesis in many more bacterial species than are known to produce cellulose. In most cases, the genes for cellulose biosynthesis are organized in an operon. Based on the organization of genes in the operons, they have been classified into four major groups (I to IV) as shown in Fig. 1 (Römling and Galperin 2015). Considerable variation is observed with respect to the morphology and amount of cellulose synthesized by different bacteria, and although the function of cellulose in bacteria is not fully understood, in many cases it is part of the biofilm.

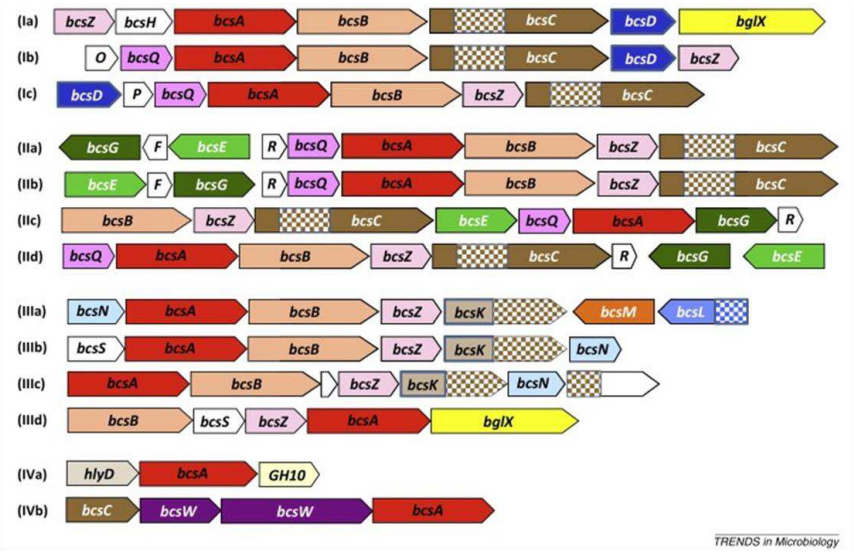

Fig. 1. Diversity of the bacterial cellulose synthase (*bcs*) operons. The displayed operons are from *Komagataeibacter xylinus* E25 (I_a), *Dickeya dadantii* Ech703 (I_b),, *Burkholderia phymatum* STM815 (I_c), *Salmonella enterica* serovar Typhimurium (II_a), *Pseudomonas putida* KT2440 (II_b), *Burkholderia mallei* ATCC 23344 (II_c), *Chromobacterium violaceum* ATCC 12472 (II_d), *Agrobacterium fabrum* C58 (III_a), *Methylobacterium extorquens* PA1 (III_b), *Azospirillum lipoferum* 4B (III_c), *Acidiphilium cryptum* JF-5 (III_d), *Nostoc punctiforme* PCC 73102 (IV_a), and *Nostoc* sp. PCC 7120 (IV_b). This figure is from Römling and Galperin 2015, and is used with permission of Elsevier.

Cellulose biosynthesis is most extensively studied in the acetic acid bacteria, mainly because of the amount and nature of the cellulose produced by *Gluconacetobacter*. In general, these bacteria are found on the surface of fruits and other locations where there is an abundant amount of sugars. In fact, the acetic acid bacterium (*G. intermedium* NEDO-01), which we currently use for the production of cellulose nanofibers, was isolated from fruits grown in Hokkaido (Kose et al. 2013). In many cases, cellulose synthesized by *Gluconacetobacter* is called bacterial cellulose (BC), and it has a dense three-dimensional network structure consisting of nanofibers (Fig. 2). The main characteristics of BC synthesized by acetic acid bacteria are as follows: (1) lignin, hemicellulose-free, (2) hierarchical assembly of nanofiber (Penttilä et al. 2018), (3) developed three-dimensional network structure, (4) high mechanical strength (high Young's modulus and tensile strength), (5) high biodegradability, (6) high biocompatibility, and (7) high water retention. Because of these characteristics, and the ability to produce it in large amounts, BC is used in making a variety of products, including speaker acoustic diaphragms (Nishi et al. 1990), artificial blood vessels (Klemm et al. 2001; Zang et al. 2015), wound dressings (Fontana et al. 1990; Portela et al. 2019), high-strength transparent materials (Yano et al. 2005; Nogi et al. 2006b, a; Ifuku et al. 2007), display devices (Shah and Brown 2005), and capacitors (Wang et al. 2016).

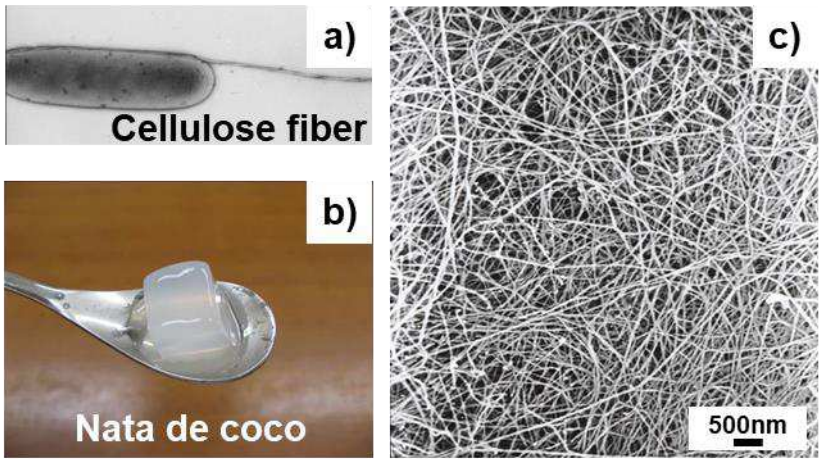

Fig. 2. (a) TEM image of *G. xylinus* cell producing a cellulose ribbon. (b) Nata de coco. (c) SEM image of lyophilized Nata de coco showing cellulose fibrils.

Cellulose is an extracellular polysaccharide and, in general, its biosynthesis involves three steps: (1) polymerization, (2) translocation, and (3) assembly or aggregation of glucan chains/crystallization (Ross et al. 1991). In Gram-negative bacteria, polymerization occurs in the cytosolic domain of the inner membrane-localized cellulose synthase, and nascent glucan chains are translocated through the inner membrane, periplasm, and outer membrane before they assemble or aggregate into higher-order structures. In *Gluconacetobacter*, the glucan chains assemble in a stepwise manner just outside the cell surface to form ribbons of crystalline cellulose I. Brown et al. visualized a linear array of particles and pores in the cell envelope of *G. xylinus* following freeze-fracture electron microscopy, and identified these as sites of cellulose synthesis (Brown et al. 1976). Zaar also observed in this bacterium a linear array of pores on the lipopolysaccharide membrane beneath the cellulose ribbons by freeze-etching, and correlated these pores with cellulose production (Zaar 1979). The pores have a rim diameter of 12-15 nm and a central hole or deepening of ~3.5 nm, and these are hypothesized to be export sites of sub-elementary fibrils (Zaar 1979). In *G. xylinus*, the average frequency of the pores is 3.8 per 100 nm, and so 50–100 pores are believed to exist along the long axis of a cell (Brown et al. 1976; Zaar 1979).

Fine structure of the cellulose ribbon was analyzed by transmission electron microscope (TEM) following incubation of *Gluconacetobacter* in medium with Calcofluor White, a fluorescent brightener (Benziman et al. 1980; Haigler et al. 1980; Haigler and Chanzy 1988). Fibers with a width of 1.5 nm were frequently observed, and it was suggested that fibers (sub-elementary fibrils) having a width of 1.5 nm were the first form of cellulose to be secreted out. Low molecular weight compounds such as fluorescent brighteners and cellulose derivatives such as carboxymethylcellulose (CMC) bind to the surface of cellulose fibers and prevent the formation of large bundles of microfibrils. Using these compounds, it was hypothesized that in *Gluconacetobacter* the assembly of cellulose microfibrils and ribbon occurs in a stepwise and hierarchical manner in the extracellular space (Fig. 3), and yet this

process is described as cell-directed because the mutual orientation and association of glucan chains, aggregates, microfibrils, bundles, and ribbons is clearly governed by the original pattern of extrusion sites (Ross et al. 1991). The linear assembly of pores on the cell surface (sites from which cellulose is secreted out, and corresponding to cellulose-synthesizing sites) that gives rise to a microfibril is referred to as a terminal complex (TC), and in the case of *Gluconacetobacter*, three pores are suggested to form a terminal complex (Brown 1996; Mehta et al. 2015). Furthermore, the cellulose ribbon produced by *Gluconacetobacter* exhibits a twist, suggesting that the cells undergo rotation during cellulose synthesis (Fig. 2a).

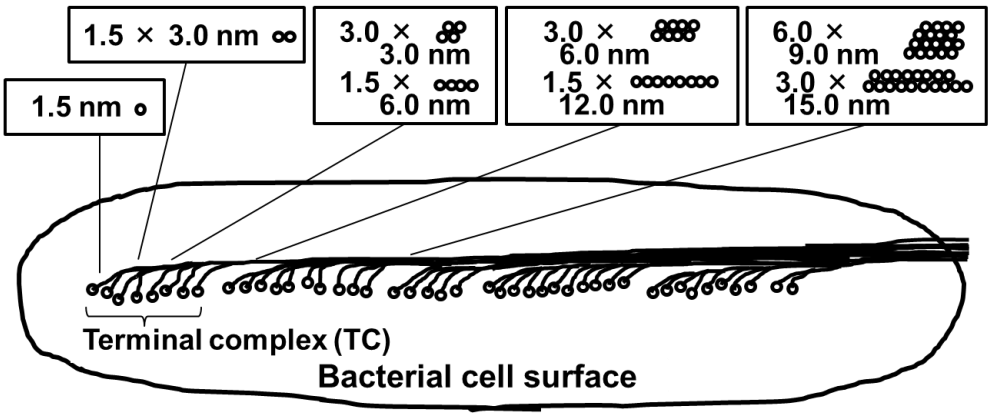

Fig. 3. Generalized model of ribbon assembly in *Gluconacetobacter*. The boxes show possible packing arrangements of the 1.5-nm tactoidal aggregates. This figure is reproduced from Ross et al. 1991, and is used with permission of American Society for Microbiology.

Using a combination of direct-staining of reducing ends of cellulose chains and microdiffraction-tilting electron crystallographic analysis, Koyama et al demonstrated that the reducing ends of growing glucan chains in the cellulose ribbon of *Gluconacetobacter* point away from the bacterium, suggesting that polymerization of glucose residues takes place at the nonreducing end of the growing glucan chains (Koyama et al. 1997). Thus, all the glucan chains point in the same direction for the ‘‘parallel-up’’ packing in unit cells of cellulose I. This packing arrangement is also consistent with the mechanism of cellulose synthesis suggested by the structure of cellulose synthase from *R. sphaeroides* (Morgan et al. 2013). Considering that TCs are present along the longitudinal axis of *Gluconacetobacter* cells and they participate in synthesis of the cellulose ribbon, it has been possible to localize a few

proteins to these cellulose-synthesizing complexes using electron and fluorescence microscopy. BcsB was the first protein that was localized to the TCs in *Gluconacetobacter* by immunolabeling of freeze-fracture replicas followed by electron microscopy (Fig. 4) (Kimura et al. 2001; Sun et al. 2017). The localization of BcsA (Fig 5), BcsD (Figs. 5 and 6), and Ccp (Fig. 7) to the longitudinal axis of bacterial cells was also demonstrated by fluorescence microscopy, suggesting that these proteins are present in the TCs of *Gluconacetobacter* (Sunagawa et al. 2013; Sun et al. 2017).

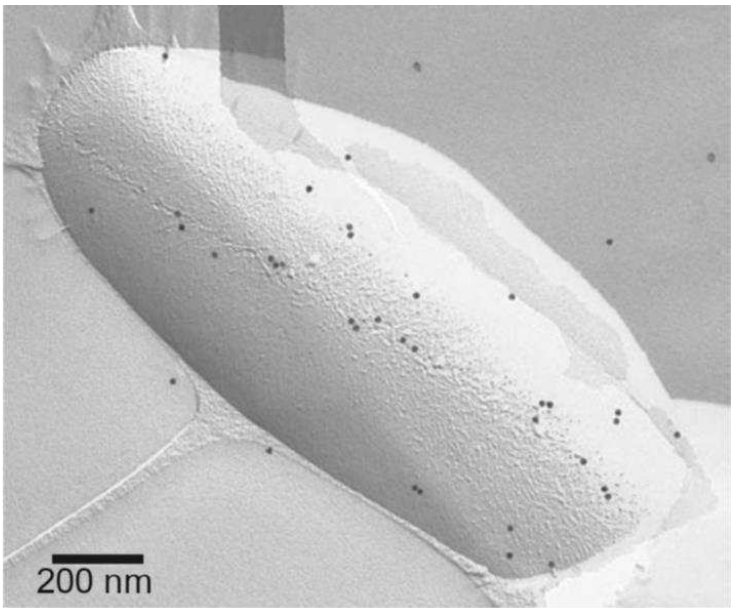

Fig. 4. Labeling of *Gluconacetobacter xylinus* ATCC 53524 with colloidal gold-bound antibody against BcsB. A linear pattern of labeling is observed despite non-specific labeling. This figure is from Sun et al. 2017, and is used with permission of Springer Nature.

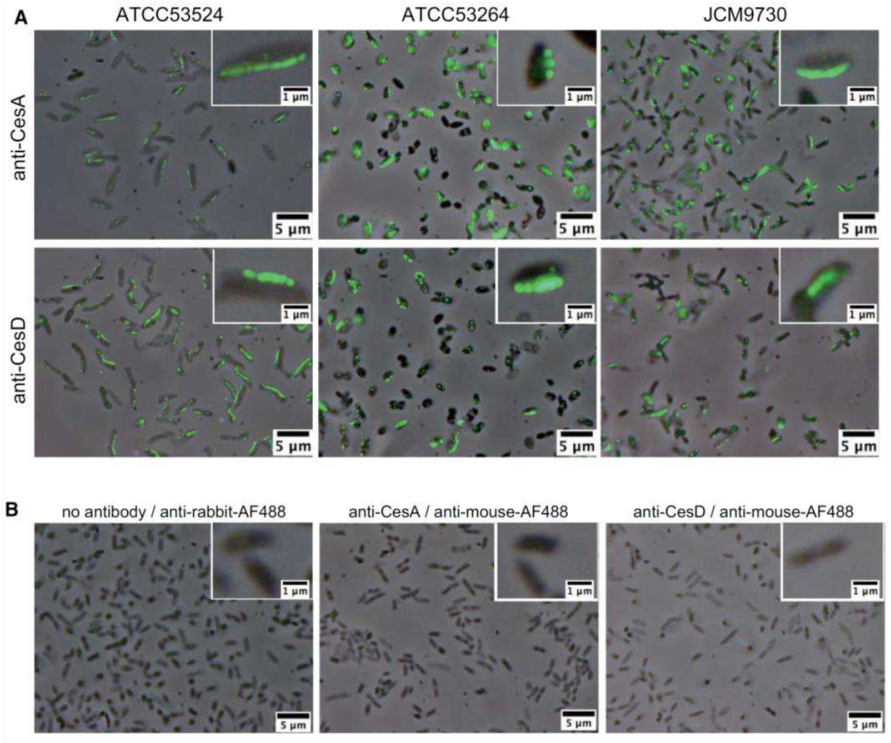

Fig. 5. Fluorescence micrographs of *Gluconacetobacter* cells following immunolabeling with antibodies against BcsA (= CesA) and BcsD (= CesD). The phase-contrast s and epi-fluorescence images are merged. A Cells from three different strains (ATCC 53524, ATCC 53264, and JCM 9730) were labeled using an identical protocol.. Insets show images at higher magnification. B Control experiments using strain ATCC 53524. Combination of primary and secondary antibodies used is as indicated. Almost no labeling was found.. This figure is from Sun et al. 2017, and is used with permission of Springer Nature.

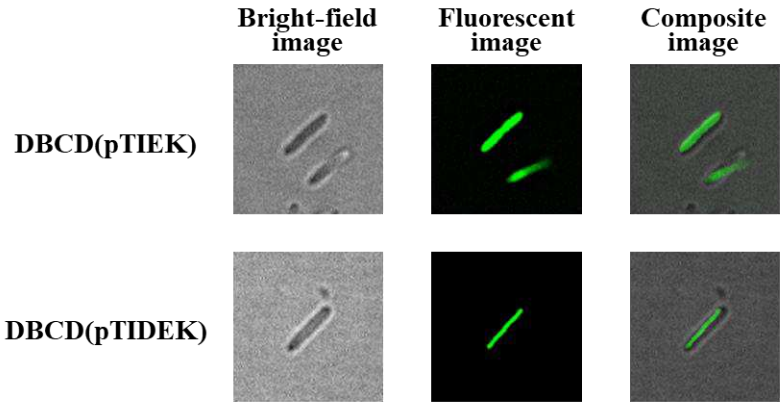

Fig. 6. Labeling of the *bcsD*-knockout mutant (DBCD) of *Gluconacetobacter* expressing native EGFP (pTIEK) or the BcsD-EGFP-fusion protein (pTIDEK). This figure is from Sunagawa et al. 2013, and is used with permission of Elsevier B.V.

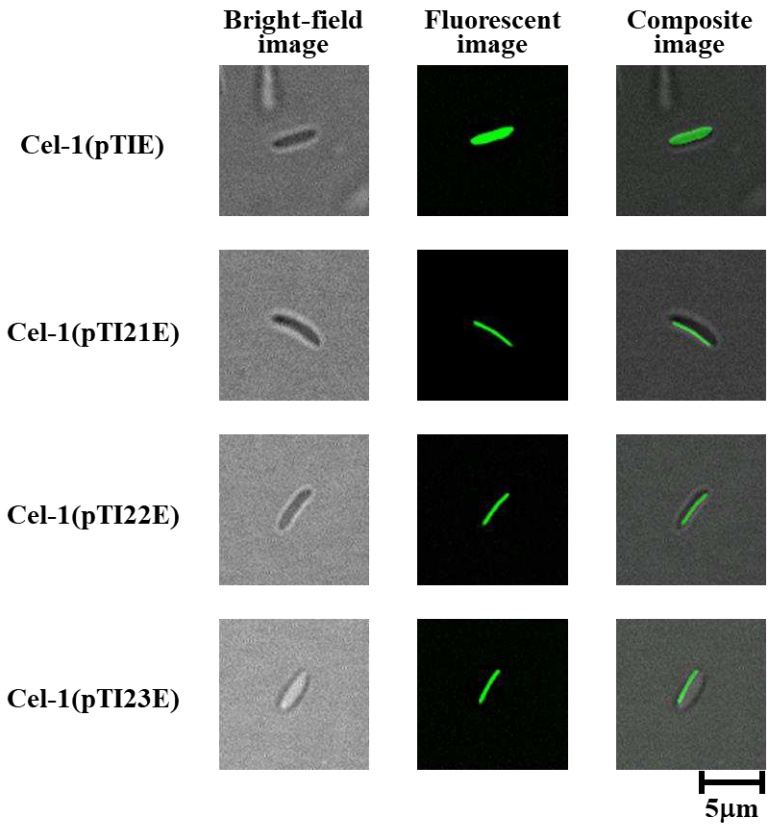

Fig. 7. Labeling of *Gluconacetobacter* with enhanced green fluorescent protein (EGFP) [Cel-1(pTIE)] or Ccp-EGFP fusion protein [Cel-1(pTI21E), Cel-1(pTI22E), and Cel-1(pTI23E)]. This figure is from Sunagawa et al. 2013, and is used with permission of Elsevier B.V.

Figures 4 – 7 show the presence of BcsA, BcsB, BcsD, and Ccp along the longitudinal axis of a cell of *Gluconacetobacter*, whereby the linear arrangement of these proteins matches with the linear arrangement of TCs in these bacteria, suggesting that these proteins are part of the cellulose-synthesizing machinery present along the same axis. However, so far it was unclear as to how the TCs line up linearly along the longitudinal axis in these bacteria. Recently, Nicolas et al. studied cellulose-synthesizing *Gluconacetobacter* in a frozen-hydrated, near-native state by cryo-electron tomography and focused-ion-beam milling, and observed a new cytoskeletal structure called the cortical belt, adjacent to the inner membrane and below the site where cellulose is seen emerging from cells (Fig. 8) (Nicolas et al. 2021). The cortical belt was not observed in other cellulose-producing bacteria, such as *A. tumefaciens* and *E. coli* 1094. Since these other bacterial species do not produce organized cellulose ribbons, Nicolas et al. proposed that the cortical belt holds the cellulose-synthesizing

complex in a row to form higher-order cellulose structures such as sheets and ribbons (Nicolas et al. 2021).

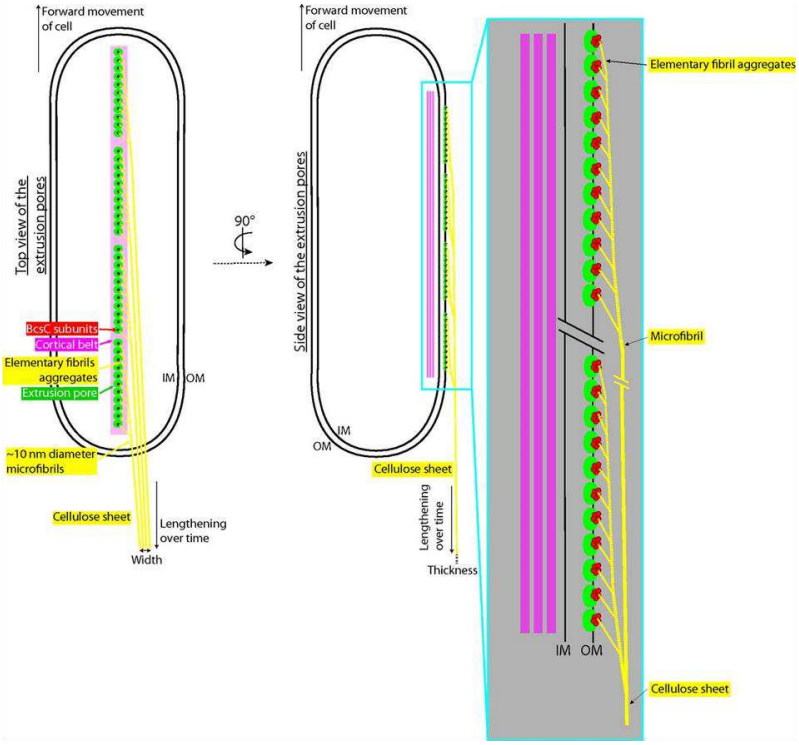

Fig. 8. Updated cell-directed hierarchical model. Top (left) and side (right) views of a *G. hansenii* cell showing the different aggregation steps leading to a cellulose sheet, how microfibrils contribute to sheet width, and the role of the cortical belt. In this model, clusters of 11 extrusion pores are depicted (green circles); the real numbers and distribution are unknown. Each extrusion pore is presented as comprising 5 BcsC subunits (red circles); the actual number is not known. On the right is a magnified view of the line of 11 extrusion pores, each hypothesized to extrude an aggregate of multiple elementary fibrils (yellow dashed lines). All aggregates then coalesce to form a microfibril of increasing thickness as it incorporates an increasing number of elementary fibril aggregates. These microfibrils then stack together, contributing to the width of the cellulose sheet (Nicolas et al. 2021: W. J. Nicolas, D. Ghosal, E. I. Tocheva, E. M. Meyerowitz, G. J. Jensen J. Bacteriol. 203, e00371-20 DOI: 10.1128/JB.00371-20). Published by The American Society for Microbiology.

Cellulose synthase (BcsA-BcsB)

Cellulose synthase is the key enzyme in cellulose biosynthesis. The first purified form of this enzyme from *Gluconacetobacter* showed that it is made of two different-sized polypeptides that were later identified as BcsA and BcsB (Lin and Brown, Jr. 1989). BcsA was identified as the UDP-glucose-binding and catalytic subunit (Lin et al. 1990) but the function of BcsB was not fully understood until the structure of cellulose synthase (BcsA-

BcsB) from *R. sphaeroides* was determined (Morgan et al. 2013). BcsA is a transmembrane protein that is present in the inner membrane, and it contains a glycosyltransferase family 2 (GT-2) domain, a PilZ domain, and eight transmembrane helices (TMHs).

The first structure of cellulose synthase was determined following expression of the *R. sphaeroides bcsA* and *bcsB* genes in *E. coli*, and purification and crystallization of the catalytically active BcsA-BcsB complex (Morgan et al. 2013). BcsA and BcsB from *R. sphaeroides* form a 1:1 stoichiometric complex (Morgan et al. 2013), similar to what is observed in purified cellulose synthase from *Gluconacetobacter* (Chen and Brown 1996). The BcsA-BcsB complex of *R. sphaeroides* has a membrane-spanning domain, a large cytoplasmic loop of BcsA that contains the GT domain, and a periplasmic domain made mostly of BcsB (Morgan et al. 2013). A helix of BcsB spans the inner membrane; at the same time, BcsB also interacts in some manner with the outer membrane (Kimura et al. 2001; Sun et al. 2017).

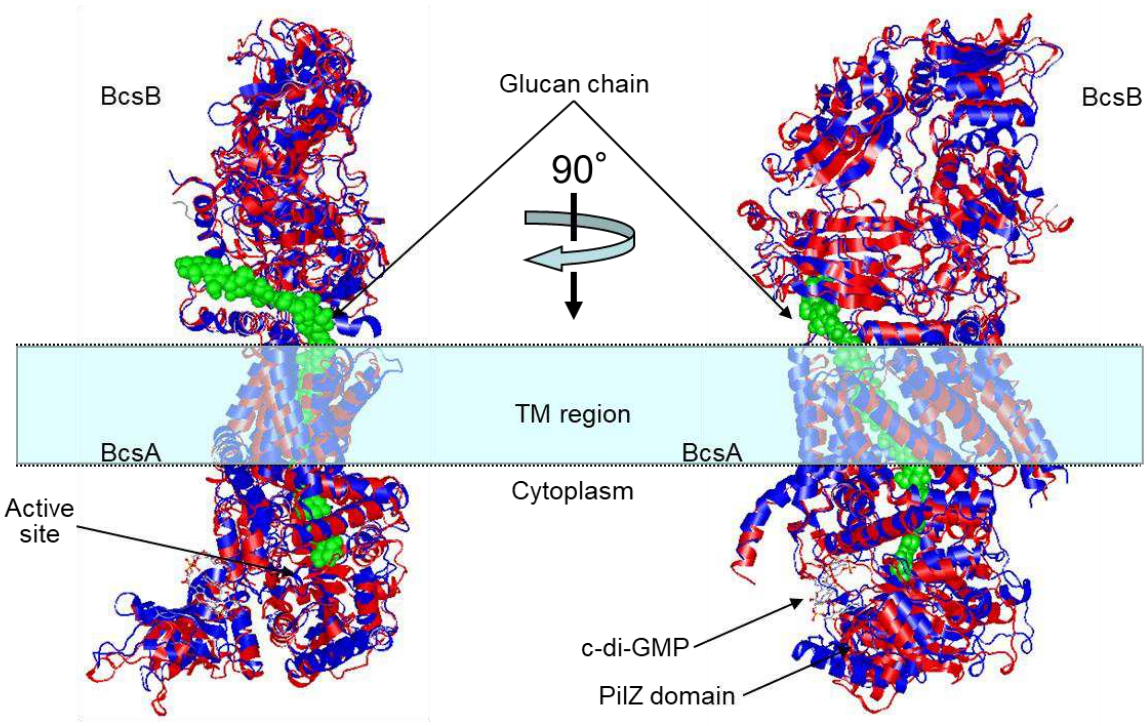

Fig. 9. Model structure of the BcsA-BcsB complex from *G. hansenii* ATCC 23769 (red) predicted by Phyre2 (http://www.sbg.bio.ic.ac.uk/~phyre2/html/page.cgi?id=index) using BcsA-BcsB complex (PDB: 5EJ1, blue) from *R. sphaeroides* as a template.

We modeled the structure of the BcsA-BcsB complex from *Gluconacetobacter* using Phyre2 (http://www.sbg.bio.ic.ac.uk/~phyre2/html/page.cgi?id=index) with the structure of BcsA-BcsB from *R. sphaeroides* (PDB: 5EJ1) as a template. Figure 9 shows that the modeled structure of the *G. hansenii* ATCC 23769 BcsA-BcsB complex is quite similar to the BcsA-BcsB complex of *R. sphaeroides*. Alignment of the amino acid sequences and secondary structures of BcsA from *R. sphaeroides* and *G. hansenii* ATCC 23769 shows that the active site in BcsA of *G. hansenii* exists between amphipathic interface (IF) helices 1 and 2, similar to what is observed in BcsA from *R. sphaeroides* (Fig. 10). The three aspartic acid residues in the conserved D,D,D,Q-X-X-R-W motif identified in cellulose synthases and other b-glycosyltransferases (Saxena et al. 1995) correspond to D171, D221, and D316 of the *G. hansenii* ATCC 23769 BcsA. The amino acids residues in the Q-X-X-R-W motif of *G. hansenii* ATCC 23769 BcsA correspond to Q352, R353, V354, R355, and W356, and these residues are present in IF2 (Fig. 10).

The structure of the BcsA-BcsB complex from *G. hansenii* ATCC 23769 is determined at 23.4 Å resolution using negative stain images (Fig.11) (Du et al. 2016). The structure reveals that BcsA-BcsB of *G. hansenii* ATCC 23769 is quite similar to BcsA-BcsB from *R. sphaeroides*. Both the active site involved in substrate binding, and the PilZ domain required for c-di-GMP binding mapped to the cytosolic region in the BcsA-BcsB complex of *G. hansenii* ATCC 23769. Importantly, this study shows that the BcsA-BcsB complex in crystalline cellulose-producing bacteria and non-crystalline cellulose-producing bacteria share a conserved catalytic domain and similar membrane translocation components (Du et al. 2016).

Morgan et al. reported that the binding of bis-(3',5')-cyclic-di-guanosine monophosphate (c-di-GMP) to the PilZ domain of BcsA results in a large migration of the gating loop, such that the active site can access (or has more access to) the substrate

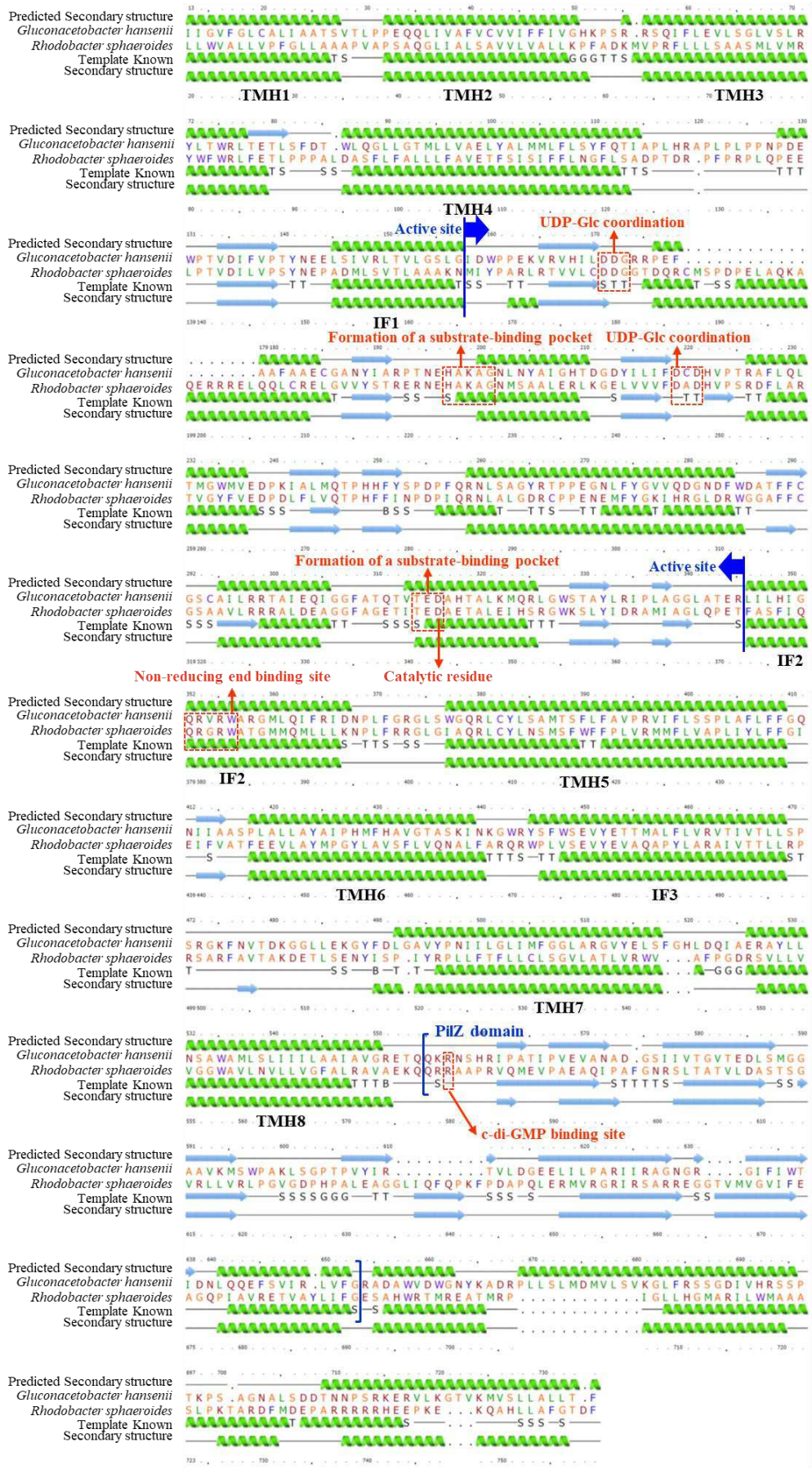

Fig. 10. Modeling of BcsA from *G. hansenii* ATCC 23769 by Phyre2 (http://www.sbg.bio.ic.ac.uk/~phyre2/html/page.cgi?id=index) using BcsA from *R. sphaeriides* as a template.

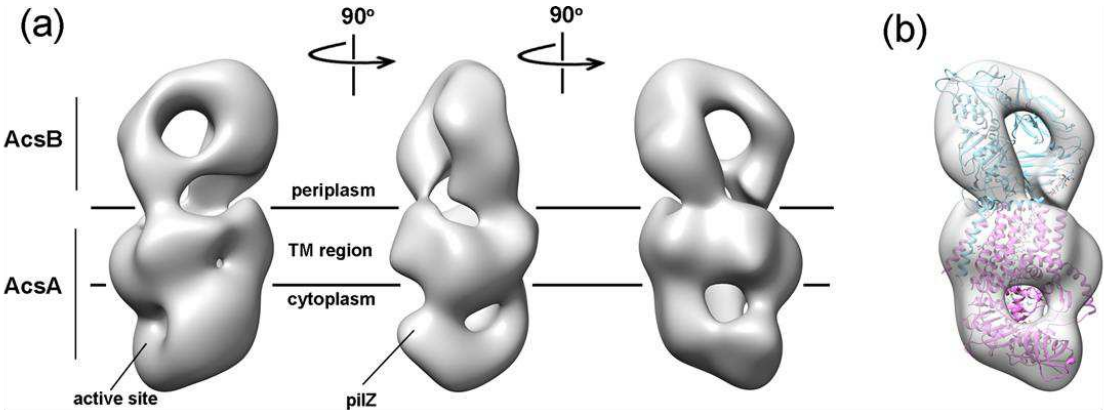

Fig. 11. 3D reconstruction of negatively stained BcsA-BcsB complex (=AcsAB) from *G. hansenii* ATCC 23769 at 23.4 Å. (a) Three side views of 3D reconstructed model of BcsA-BcsB complex. The volume of BcsA is composed of membrane embedded TM region and a large cytosolic region. The active site responsible for substrate binding and PilZ domain required for activator c-di-GMP binding are mapped in the cytosolic region. The density of BcsB sits on the top of BcsA. The cytoplasmic membrane boundaries are represented by black lines. (b) The BcsA-BcsB EM density map was docked with crystal structure of BcsA-BcsB (PDB: 4HG6). BcsA and BcsB are shown in orchid and cyan ribbon representatives, respectively. The translocating glucan co-crystallized with BcsA-BcsB is indicated in cyan sphere (Du et al. 2016: J. Du, V. Vepachedu, S. Hyun Cho, M. Kumar, and B. T. Nixon PLoS ONE 11, e0155886 DOI: 10.1371/journal.pone.0155886).

UDP-glucose (Morgan et al. 2014). Glucose is transferred from UDP-glucose to the non-reducing end of the glucan chain, which is the growing end (Koyama et al. 1997). Based on the 2-fold helical symmetry of the glucan chain in cellulose, it would appear that UDP-glucose alternately approaches from two opposite sides of the non-reducing terminal residue of the extending glucan chain. Instead, a mechanism is proposed in which the glucose residue, immediately after the rearrangement reaction, rotates with respect to the glycosidic bond and is inverted with respect to the adjacent residue on the reducing end side (Morgan et al. 2016).

Knott et al. confirmed this proposed mechanism by molecular simulation (Fig. 12) (Knott et al. 2016). A multi-scale simulation applying quantum chemistry analyzed the three-dimensional structural changes, including the activation energy of the rearrangement reaction and the proton transfer along the reaction coordinates (Knott et al. 2016). The proposed synthesis cycle is as follows (Knott et al. 2016): Glycosyl transfer can add the glucose moiety from UDP-glucose in the same orientation as the acceptor glucose (‘same side’, with the hydroxymethyl of both rings on the same side) or in the opposite orientation (‘opposite side’).

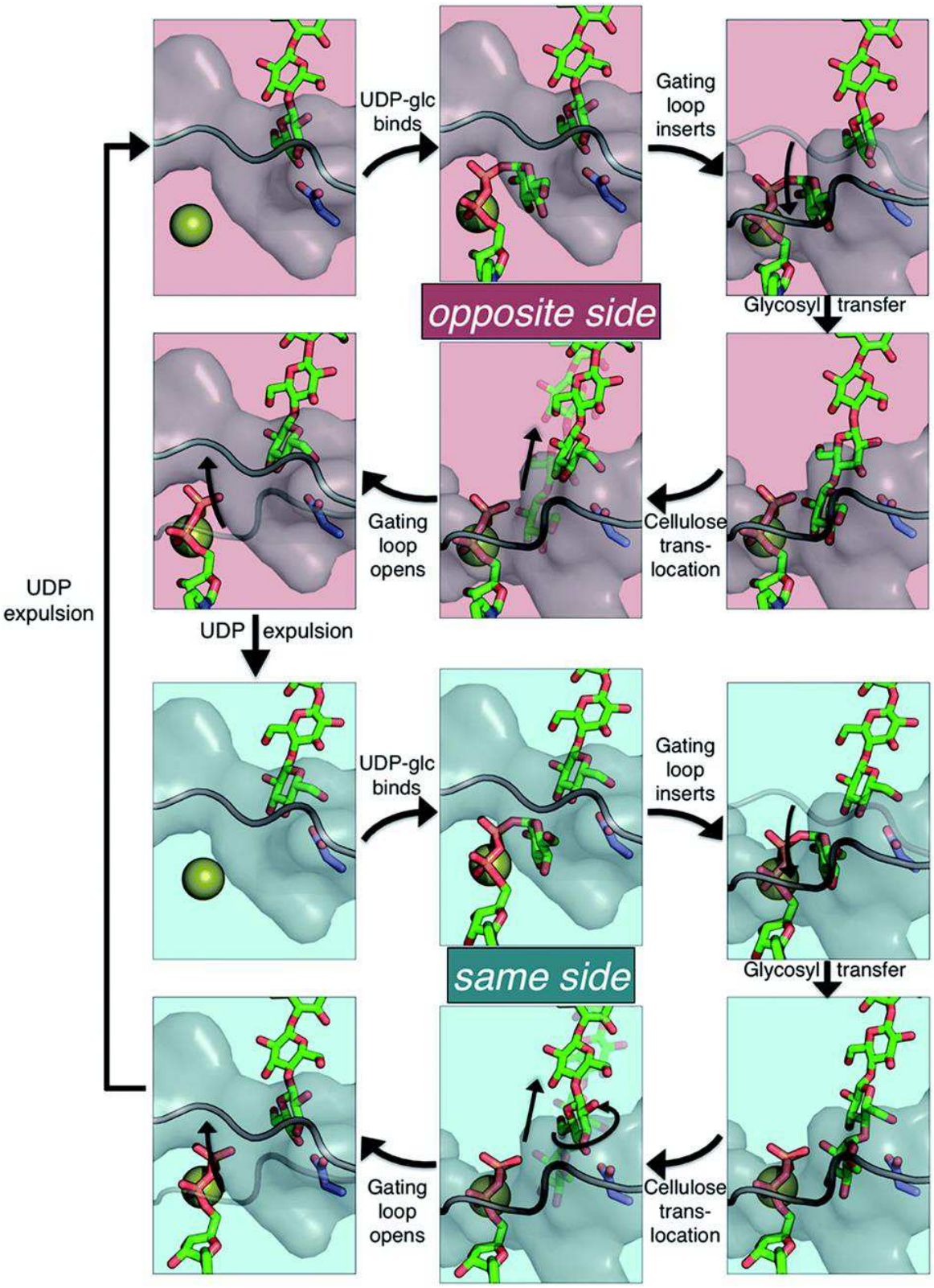

Fig. 12. The hypothesized processive cycle of the bacterial cellulose synthase (Knott et al. 2016: B. C. Knott, M. F. Crowley, M. E. Himmel, J. Zimmer and G. T. Beckham, Chem. Sci., 2016, 7, 3108 DOI: 10.1039/C5SC04558D). Published by The Royal Society of Chemistry.

Basically, the same process occurs for both the 'opposite side' (top six panels) and the 'same side' (bottom six panels) portions of the cycle: (upper left) gating loop is open and active site is empty; (upper middle) UDP-glucose binds in the active site; (upper right) the gating loop inserts into the active site; (lower right) glycosyl transfer produces an elongated cellulose chain and UDP product; (lower middle) cellulose translocation moves the chain into the transmembrane tunnel; (lower left) gating loop opens facilitating UDP product expulsion (Fig. 12). In addition, it is suggested that the rotation of glucose residues immediately after the rearrangement reaction proceeds thermodynamically due to interaction with the surrounding aromatic side chains, and the up-and-down movement of finger helix that guides the cellulose molecular chain in the transmembrane (TM) direction is thermodynamically possible (Knott et al. 2016).

The structure of the PilZ domain of BcsA from *G. hansenii* ATCC 23769 (Fujiwara et al. 2013) is similar to the PilZ domain of BcsA from *R. sphaeroides* (Morgan et al. 2013) (Fig. 13). The arginine (R580) within the TM8–β-barrel linker and glutamine (E371) residues in BcsA from *R. sphaeroides*, which are responsible for the regulation of cellulose synthesis, are conserved and correspond to R557 and E344 in BcsA from *G. hansenii* ATCC 23769 (Fig. 10). The similarities in the PilZ domain of BcsAs from *R. sphaeroides* and *G. hansenii* suggests that cellulose synthase is regulated by a similar mechanism in these two bacteria.

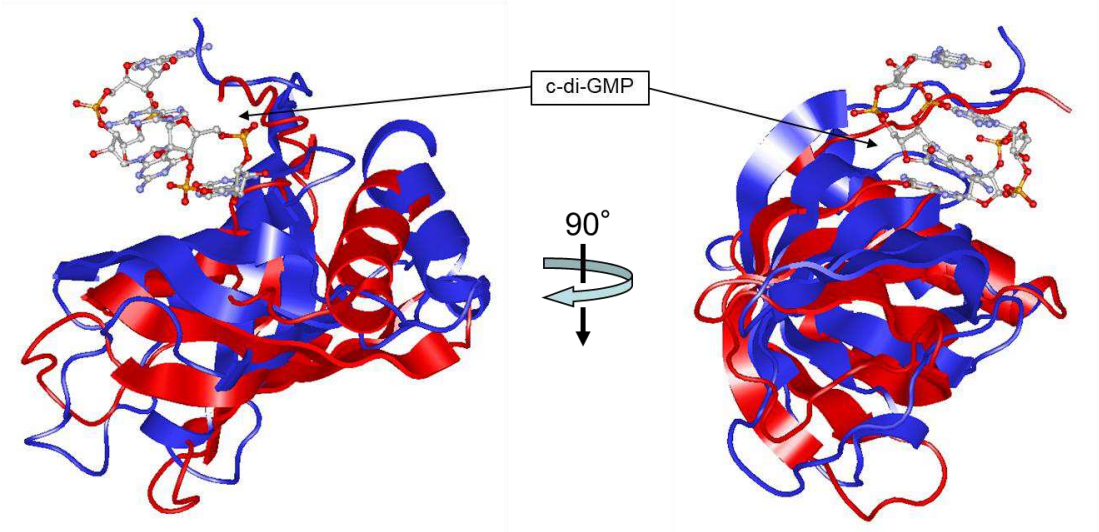

Fig. 13. Structures of PilZ domain of BcsAs from *G. hansenii* ATCC 23769 (PDB: 4I86, red) and *R. sphaeroides* (PDB: 4P00, blue).

The structure of BcsB in the *R. sphaeroides* BcsA-BcsB complex shows the presence of a periplasmic BcsB domain (function unknown) and one transmembrane domain on the C-terminal side (Morgan et al. 2013). The BcsB domain consists of two cellulose-binding domains (CBDs 1 and 2) and two flavodoxin-like domains (FDs 1 and 2). The CBDs are positioned at a 45° angle relative to one another, and stabilized by disulfide bonds. CBD1 has a conserved amino acid sequence (H159, R160, I161, L171, and W172) similar to that of a bacterial CBD which forms a complex with glucuronic acid dimers, suggesting that this region could be involved in translocation of a glucan chain (Morgan et al. 2013). BcsB is absolutely required for BcsA catalytic activity. Studies in *R. sphaeroides* identified the BcsB C-terminal transmembrane helix and the preceding amphipathic helix as being necessary for the BcsA catalytic activity, possibly through stabilization of the transmembrane region of BcsA and completing its inner membrane transport domain (Omadjela et al. 2013). Although the stoichiometry of BcsA to BcsB is 1:1 in *Gluconacetobacter* and *R. sphaeroides*, cryo-EM studies of *E. coli* cellulose synthesizing complexes show a hexamer of BcsBs associating with a single BcsA (Abidi et al. 2021; Acheson et al. 2021).

BcsC

BcsC is the largest protein (~130 kDa) encoded by genes present in the *bcs* operon. Along with *bcsA* and *bcsB*, *bcsC* is part of the *bcs* operon in almost all bacteria. In most cases, transcription of *bcsC* follows that of *bcsA* and *bcsB*. Cellulose synthase activity is not affected in *Gluconacetobacter* mutants in which the *bcsC* gene is disrupted, but these mutants do not produce cellulose, suggesting that BcsC is an essential protein for in vivo cellulose synthesis (Saxena et al. 1994). Proteins similar to BcsC play a role in secretion of exopolysaccharides in other bacteria (Whitney and Howell 2013). BcsC has an N-terminal tetratricopeptide repeat (TPR) domain and a C-terminal pore-forming b-barrel domain. Acheson et al. determined the crystal structure of a truncated BcsC protein from *E. coli* that contains a TPR repeat, a linker

region and the complete b-barrel pore (Acheson et al. 2019). Modeling of structure of the C-terminal part of BcsC from *G. hansenii* ATCC 23769 using Phyre2 shows that the higher-order structure of *G. hansenii* BcsC is similar to the BcsC from *E. coli* (Fig. 14). BcsC is localized in the outer membrane and periplasmic space, and in *E. coli* it is estimated that one phosphoethanolamine-modified glucan chain (pEtN-cellulose) is excreted from the cells through the β-barrel channel (Acheson et al. 2019). It is not known if BcsC in *Gluconacetobacter* transports a single glucan chain or a bundle of glucan chains (sub-elementary fibril).

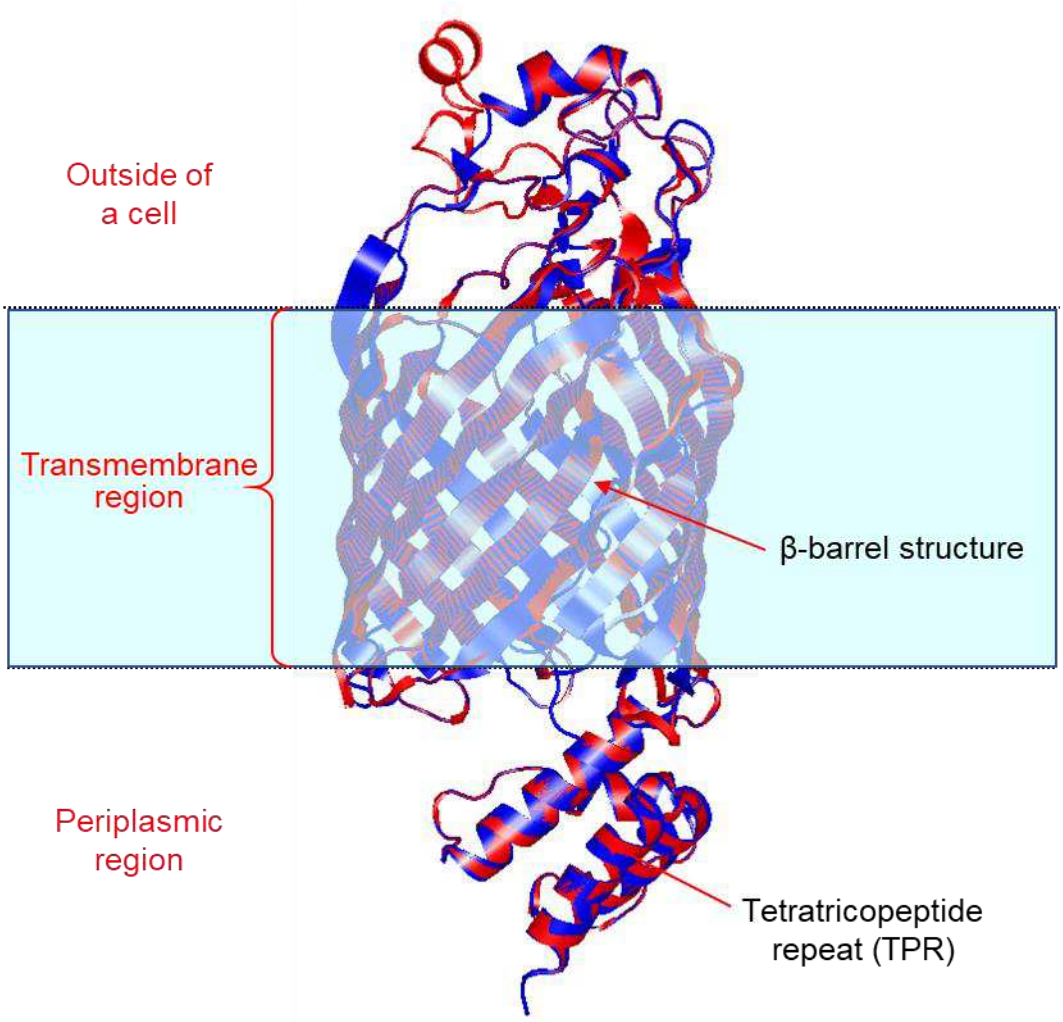

Fig. 14. Model structures of BcsC from *G. hansenii* ATCC 23769 (red) obtained using Phre2 and BcsC (PDB: 6TZK, blue) from *E. coli* as the template.

The TPRs towards the C-terminal side of BcsC are composed of two antiparallel α-helices connected by a turn. These TPRs are stacked on each other to form a superhelical structure, something observed in other TPR-containing proteins (D'Andrea and Lynne 2003). Figure 15 shows the TPR domain of BcsC from *Enterobacter* sp. CJF-002 (Nojima et al. 2017). The hinge (turn) between α5 and α6 allows the C-terminal part to move, suggesting that this region may be involved in extrusion of the glucan chain.

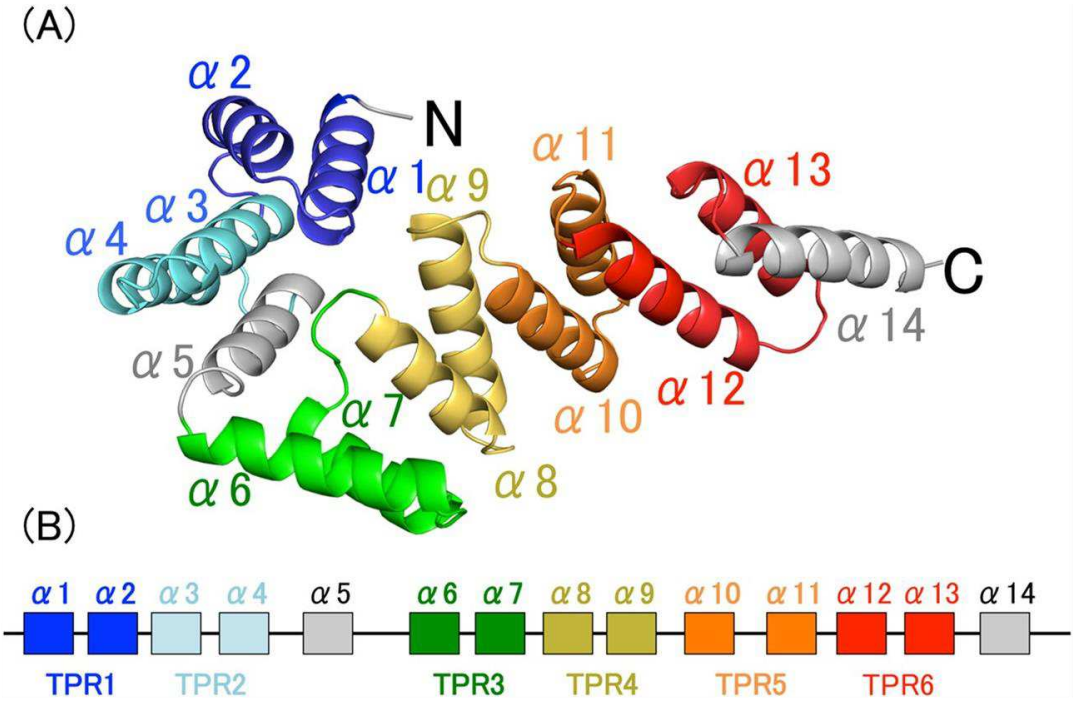

Fig. 15. The structure of BcsC-TPR(N6) from *Enterobacter* CJF-002 (A) BcsC-TPR(N6) is composed of six TPR motifs (colored blue, light blue, green, yellow, orange, and red) and two unpaired α-helices (gray). (B) Schematic diagram of the secondary structure of BcsC-TPR(N6). The boxes indicate α-helices and the lines indicate turns. The color scheme is the same as in (A). (Nojima et al. 2017: S. Nojima, A. Fujishima, K. Kato, K. Ouchi, N. Shimizu, K. Yonezawa, K. Tajima, and M. Yao. Sci Rep 2017, 7, 13018 DOI: 10.1038/s41598-017-12530-0). Published by Springer Nature.

BcsD

In *Gluconacetobacter*, *bcsD* follows *bcsC*, and is the last gene in the *bcs* operon. For many years, *bcsD* was identified only in *Gluconacetobacter*, but as more bacterial genome sequences became available it was observed in *bcs* operons in a few other bacteria. Analysis of *Gluconacetobacter* mutants, where *bcsD* is disrupted, provided evidence that while BcsD is not required for cellulose synthase activity, this protein has a non-essential role in cellulose production (Saxena et al. 1994; Mehta et al. 2015). *bcsD* mutants of *Gluconacetobacter*

produce reduced amounts of native cellulose I; at the same time, they produce detectable amount of cellulose II, suggesting that BcsD probably influences assembly of glucan chains during formation of the cellulose ribbon. Interestingly, no homolog of BcsD has been identified in the protein databases and it maybe a unique protein. Although no signal sequence for translocation of this protein is identified in its amino acid sequence, biochemical analysis suggests that BcsD is present in the periplasmic space in *Gluconacetobacter* (Iyer et al. 2011).

Interestingly, the crystal structure of BcsD is the first one to be determined of a protein coded in the *bcs* operon of *Gluconacetobacter* (Hu et al. 2010). BcsD assembles into a cyclic octamer, with each subunit folded into a globular structure and exhibiting five α-helices and a four-stranded b-sheet (Fig. 16). In the BcsD octamer, two monomers interact with each other using the two N-terminal helices α1 and α2, which have a hook-like arrangement, resulting in a two-fold symmetrical assembly of a stable homodimer (Fig. 16A). The octamer, a tetramer of the dimers AB, CD, EF, and GH, exhibits a cylindrical structure along the non-crystallographic four-fold axis of symmetry, with a height of 65 Å, an outer diameter of 90 Å, and an inner diameter of ~ 25 Å (Fig. 16B).

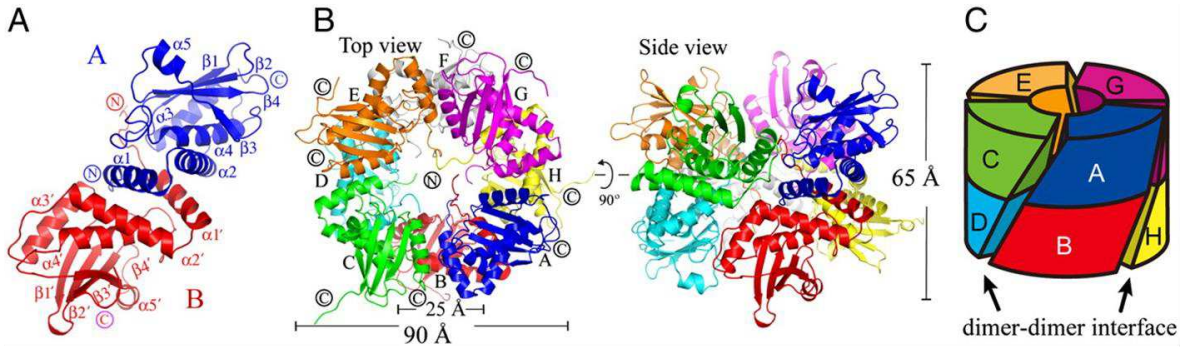

Fig. 16. Crystal structure of BcsD (=CeSD) from *G. hansenii* ATCC 23769. (A) Ribbon representation of the dimeric structure of BcsD. The two monomers are shown in blue and red, respectively. The helices and sheets are labeled, where the prime refers to the second monomer. (B) Overall structure of the BcsD octamer. The octamer structure is viewed along the 4-fold axis (top view) and the dyad axis (side view), with each monomer (A–H) shown in a different color. The N and C termini of all copies that are positioned in the center and outside of the cylinder are indicated by the circled N and C (same as in A), respectively. (C) A schematic diagram of the octamer assembly based on the side view in B. The octamer is represented by a cylinder, and monomers (A, C, E, G) and (B, D, F, H) are distributed in the top and bottom layers, respectively. The colors of each molecule correspond with those in B. The dimer–dimer interfaces are depicted with sloping rectangles, and indicated by arrows. A and B were prepared using the program PyMOL (DeLano Scientific LLC, http://pymol.sourceforge.net/) (Hu et al. 2010: S.-Q. Hu, Y.-G. Gao, K. Tajima, N. Sunagawa, Y. Zhou, S. Kawano, T. Fujiwara, T. Yoda, D. Shimura, Y. Satoh, M. Munekata, I. Tanaka, and M. Yao 2010, PNAS, 107, 17957–17961 DOI: 10.1073/pnas.1000601107). Published by the National Academy of Sciences.

The N-terminus of each subunit is present inside the octameric ring, forming four tunnel-like structures (Hu et al. 2010). To determine if glucan chains pass through these tunnel-like structures, BcsD was co-crystallized with cellopentaose (CPT), an oligosaccharide representing the glucan chain of cellulose. Results from these experiments showed that CPT was present in each of the four tunnel-like structures inside the ring (Hu et al. 2010). Whether the tunnel-like structures, formed by N-terminals of the BcsD subunits, have any role in cellulose synthesis was studied by analyzing BcsD with different lengths of N-terminal deletions (Fig. 17). These studies show that cellulose yield is reduced significantly in strains that express BcsD with N-terminal deletions, and where no tunnel-like structures are observed, suggesting that the tunnel-like structures play an important role in optimal cellulose synthesis (Hu et al. 2010).

Construction of a computerized model and molecular dynamics (MD) simulation of BcsD complexed with four cellulose chains of DP = 12 (Glc12) revealed an unexpected S-shaped pathway with a flexion region between BcsD dimers (Fig 18) in the octamer (Uto et al. 2021). Glucose residues located in the region where the pathway bends show reversible changes in ring conformation, and this phenomenon might be associated with the role BcsD plays in cellulose microfibril production (Uto et al. 2021). Furthermore, molecular modeling and molecular simulation shows that the sugar chain pathway of BcsD is much narrower than that of BcsB and BcsC, and that the cellulose chain is strongly compressed at the BcsD surface, especially in the region where the pathway bends. Since BcsD has a homogeneous octamer structure that is overall symmetrical, the cellulose chains are compressed at the BcsD surface at the same time in the four sugar chain pathways (Uto et al. 2021). The movement of nascent cellulose chains extending from four sets of BcsA-BcsB complexes is synchronized as they pass through the BcsD octamer, such that four cellulose chains are extended together during extrusion from each TC subunit (Uto et al. 2021).

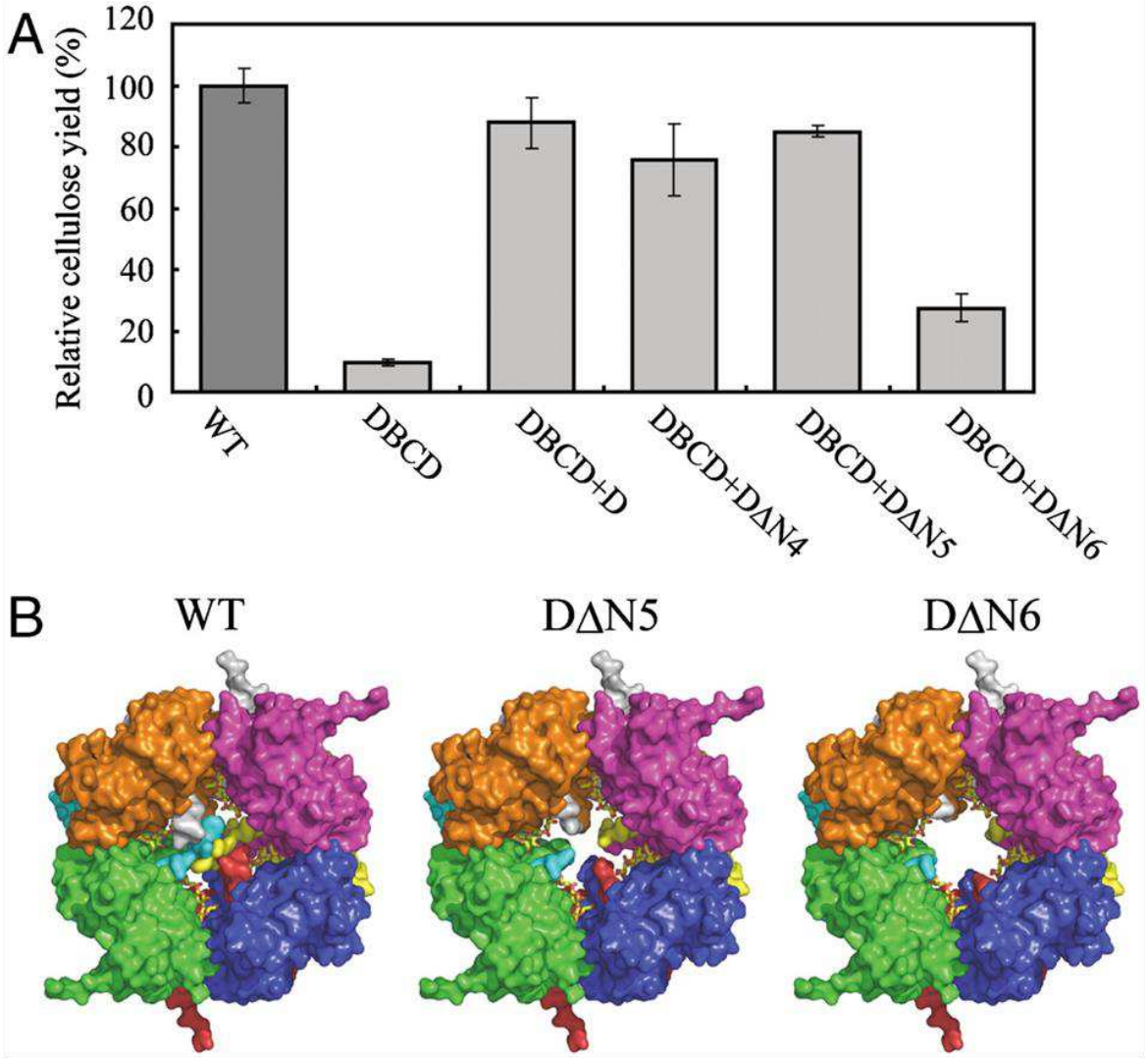

Fig. 17. Effects of deletions and mutations in *bcsD* (=*cesD*) on cellulose production. BcsDs (=CeSDs) with different lengths of N-terminal deletions were expressed in the DBCD strain of *G. hansenii* ATCC 23769. (A) The relative yield of cellulose produced by wild-type (WT), *bcsD* deletion mutant with a control vector (DBCD), *bcsD* deletion mutant with full-length Bcs*D* (DBCD+D), *bcsD* deletion mutant with BcsD in which four N-terminal residues are deleted (DBCD+DΔN4), *bcsD* deletion mutant with BcsD in which five N-terminal residues are deleted (DBCD+DΔN5), and *bcsD* deletion mutant with BcsD in which six N-terminal residues are deleted (DBCD+DΔN6).(B) Molecular surface of octamers of wild-type BcsD (WT; the three N-terminal residues are disordered), BcsD with deletion of the five N-terminal residues (DΔN5) (), and BcsD with deletion of the six N-terminal residues (DΔN6). (Hu et al. 2010: S.-Q. Hu, Y.-G. Gao, K. Tajima, N. Sunagawa, Y. Zhou, S. Kawano, T. Fujiwara, T. Yoda, D. Shimura, Y. Satoh, M. Munekata, I. Tanaka, and M. Yao 2010, PNAS, 107, 17957–17961 DOI: 10.1073/pnas.1000601107). Published by the National Academy of Sciences.

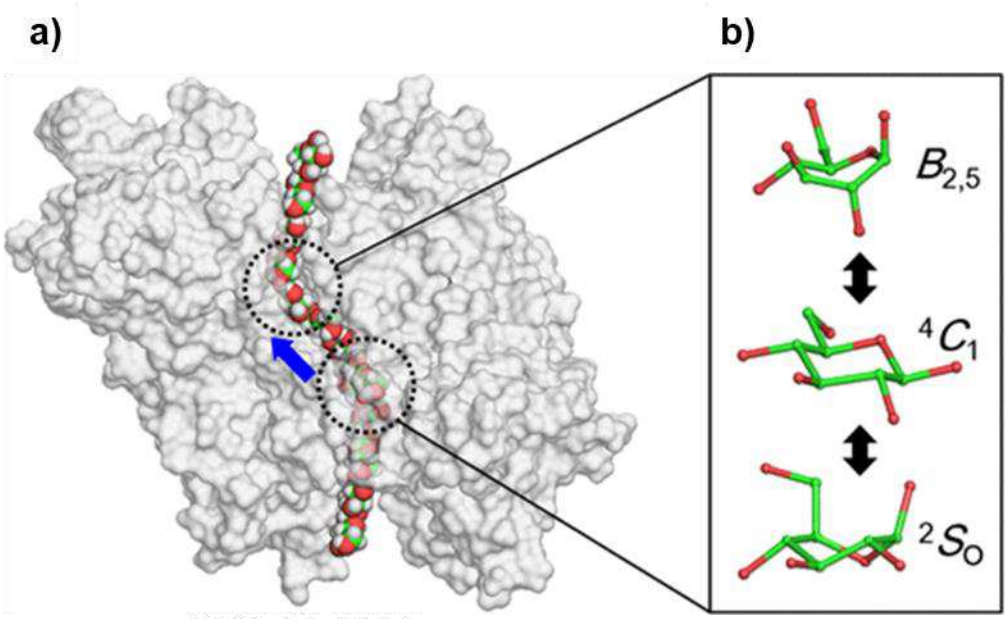

Fig. 18. A model of the BcsD(=CeSD)-G12 complex. a) Shape of a cellulose chain in the sugar chain pathway between BcsD dimers. b) Three-dimensional structural change of the pyranose ring of the glucose residues at the bend. $^4C_1$ corresponds to the original pyranose ring chair structure. This figure is from Uto et al. 2020 and is used with permission of the American Chemical Society.

Cellulose complementing factor (Ccp)

Cellulose complementing factor (Ccp) is an essential protein required for synthesis of cellulose in acetic acid bacteria. Mutation in the *ccp* gene results in loss of cellulose synthesis in *Gluconacetobacter* (Standal et al. 1994). A fusion protein of Ccp and a fluorescent protein (EGFP) was used to determine the requirement of Ccp in cellulose synthesis and its localization (Sunagawa et al. 2013). Expression of the fusion protein in a Ccp-deficient strain (Cel-1) of *Gluconacetobacter* resulted in gain of cellulose synthesis in the mutant strain, and the fusion protein was found to localize along the longitudinal axis of the cell (Fig. 7) (Sunagawa et al. 2013). More interestingly, pull-down assays revealed that Ccp directly interacts with BcsD (Fig. 19), suggesting that Ccp is part of the cellulose-synthesizing complex (Sunagawa et al. 2013). Presently, the function and structure of Ccp is not known.

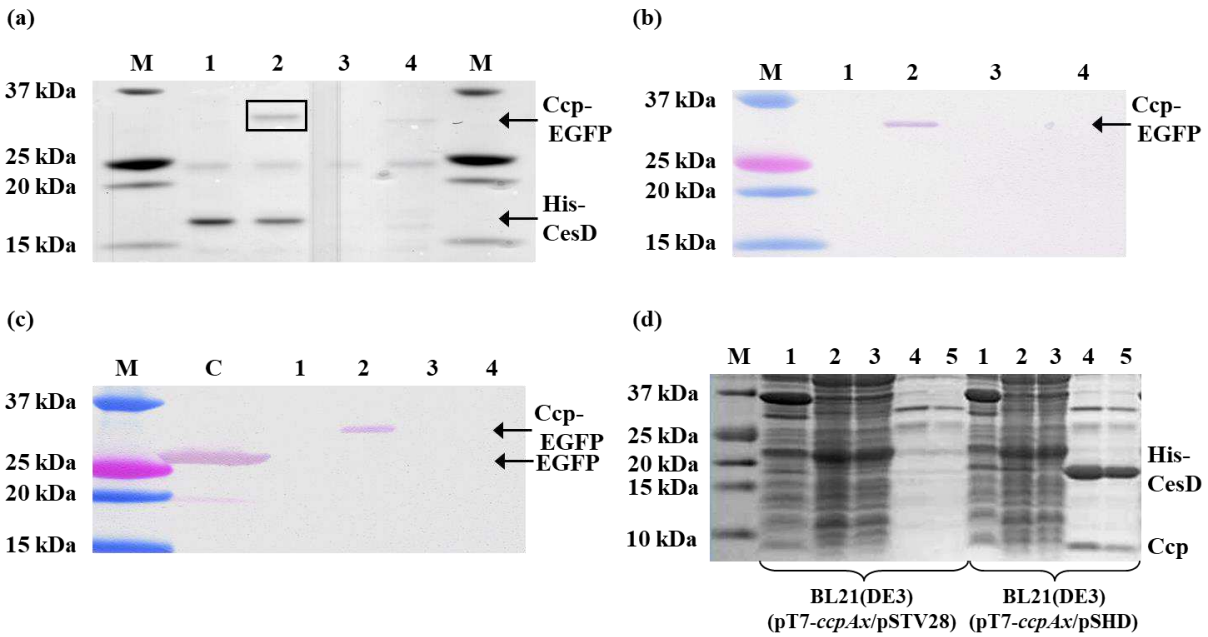

Fig. 19 Confirmation of interaction between Ccp and BcsD (CeSD) by pulldown assay. (a) SDS-PAGE gel; (b) Western blot using an anti-Ccp antibody; (c) Western blot using an anti-EGFP antibody; (d) SDS-PAGE gel. For (a), (b), and (c): M: marker; C: JM109(pTIE); lane 1: JM109(pSHD/pTIE); lane 2: JM109(pSHD/pTI23E); lane 3: JM109(pSTV28/pTI23E); 4: JM109(pSTV28/pTIE). For (d): M: marker; lane 1: debris; lane 2: crude lysate; lane 3: flow through; lane 4: elution fraction 1; lane 5: elution fraction 2. This figure is from Sunagawa et al. 2013, and is used with permission of Elsevier B.V.

Endo-glucanase (CMCax)

CMCax is an endo-type glucanase that hydrolyzes glucan chains to reduce the molecular weight, and is classified in Glycosyl hydrolase Family 8 (GH-8). In *Gluconacetobacter*, the *cmcax* gene is present upstream of the *bcs* operon, together with the *ccp* gene (Fig. 1: Ia, *bcsZ* = *cmcax*, *bcsH* = *ccp*) (Standal et al. 1994). Based on immunostaining and TEM observations, CMCax is shown to be present not only in the growth medium but also on the cell surface of *Gluconacetobacter* cells (Yasutake et al. 2006). In CMCax-deficient *Gluconacetobacter* mutants, cellulose yield is significantly reduced and the cellulose ribbon is extremely twisted compared to that produced by the wild strain, suggesting that CMCax has a function in eliminating strain and facilitating ribbon formation (Nakai et al. 2013).

GH-8 enzymes hydrolyze glycosidic linkages using general acid catalysis, and a proton donor and a nucleophile or general base are required (Alzari et al. 1996). From

sequence alignment of GH-8 enzymes, Glu57 in CMCax is suggested as a putative proton donor (Yasutake et al. 2006). Endo-glucanase (CtCelA) from *Clostridium thermocellum*, which belongs to GH-8, has five aromatic residues for sugar recognition by stacking interactions. These residues correspond to Trp132, Trp205, Tyr372, Tyr277, and Tyr369, and form five sugar-recognition subsites, –3, –2, +1, +2, and +3, respectively (Fig. 20, left) (Schmidt et al. 2002). However, residue corresponding to Tyr369 of CtCelA is not conserved in CMCax, suggesting that CMCax lacks subsite +3 (Fig. 20, right). Other endoglucanases involved in cellulose synthesis, BcsZEc from *E. coli* (Mazur and Zimmer 2011) and BcsZEn from *Enterobacter* (Sunagawa et al. 2012), are also deficient in the +3 subsite, suggesting that this structural change may have a role in cellulose synthesis.

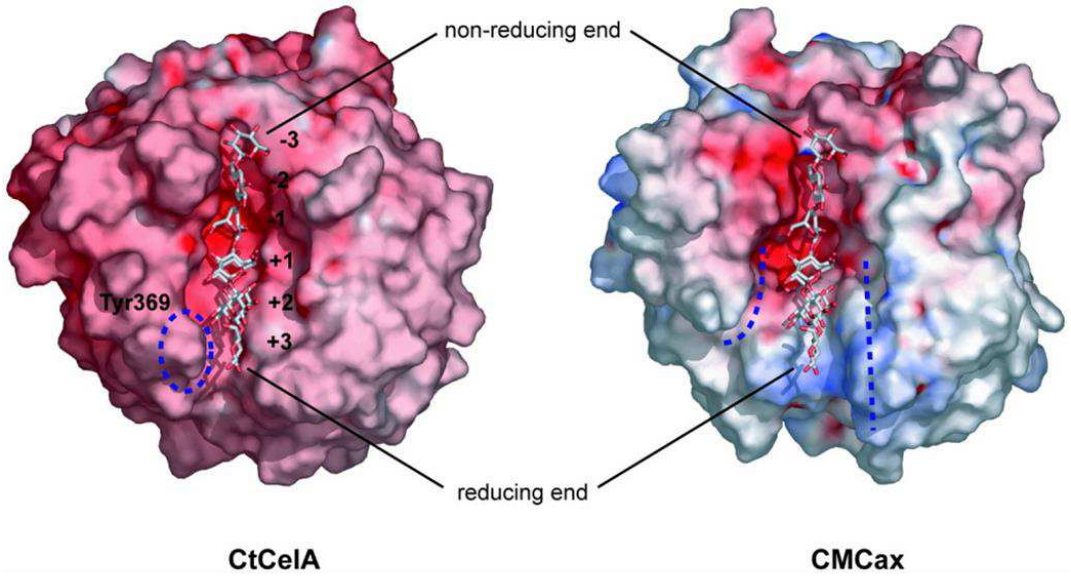

Fig. 20. Molecular surface potential representation of CtCelA (PDB code, 1kwf) and CMCax. The model of substrate in the structure 1kwf is also shown in the cleft of CMCax. The electrostatic surface potentials were generated using PyMol (DeLano Scientific LLC, http://pymol.sourceforge.net/) in absolute mode. Areas colored in white, red, and blue denote neutral, negative and positive potential, respectively. This figure is used with permission from John Wiley & Sons, Inc.

β-glucosidase (Bgl)

In *Gluconacetobacter*, the 1,4-β-glucosidase gene (*bgl*) is located downstream of the *bcs* operon (Fig. 1), and Bgl is classified in Glycosyl Hydrolase family 3 (GH-3) (Tonouchi et

al. 1997; Tajima et al. 2001; Kawano et al. 2002b).1,4-β-glucosidase from *Gluconacetobacter sucrofermentans* BPR2001 has been purified and characterized (Tahara et al. 1998a). Assays of hydrolysis using cellooligosaccharides (Glc2–Glc6) show that it is an exo-type hydrolase that hydrolyzes cellooligosaccharides longer than cellotriose from the non-reducing end (Tahara et al. 1998a).

Determination of subsite affinities show that Glc2 (cellobiose) cannot bind rigidly at the active site of 1,4-β-glucosidase to release cellobiose (Tahara et al. 1998b). Modeling of Bgl from *G. hansenii* ATCC 23769 by Phyre2 using BGL (PDB: 3AC0) from *Kluyveromyces marxianus* as a template suggests that the active site of Bgl is located near the center and is bag-shaped (Fig. 21). This suggestion corresponds with results of experiments on determination of the subsite of Bgl (Tahara et al. 1998b).

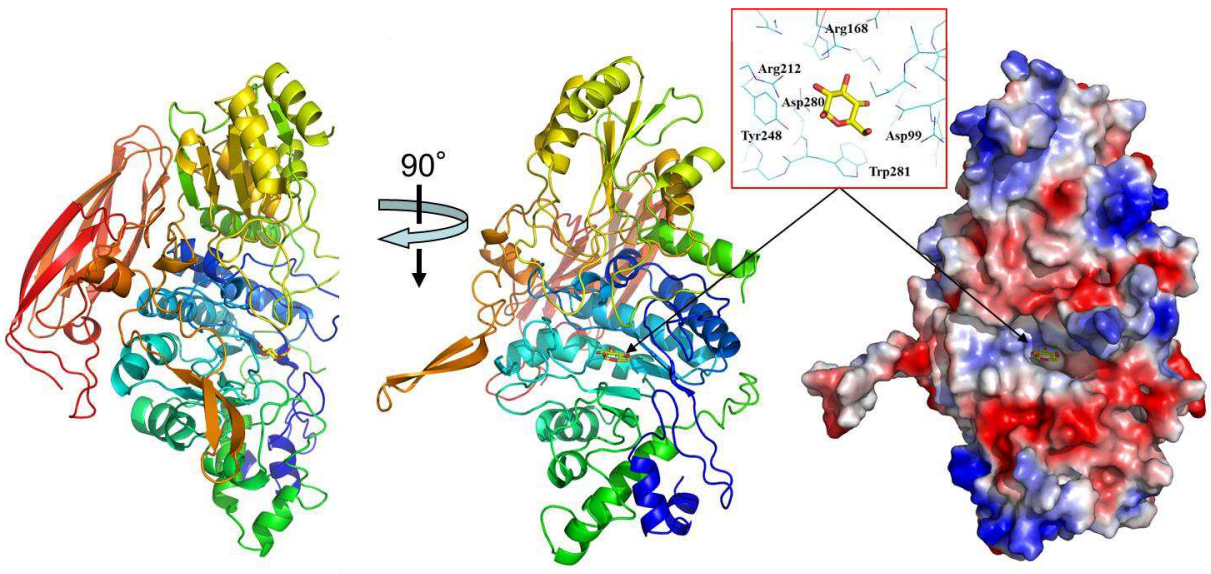

Fig. 21. Model structure of β-glucosidase (Bgl) from *G. hansenii* ATCC 23769 predicted by Phyre2 using Bgl (PDB: 3AC0) from *Kluyveromyces marxianus* as a template.

It is also known that Bgl catalyzes glycosylation reactions depending on the reaction conditions, and produces various β-glycosidic disaccharides (Kawano et al. 2008). Amongst the different disaccharides produced by Bgl, gentiobiose (β1,6-linked disaccharide of glucose) is known to induce expression of CMCax. From temporal changes in the expression of *cmcax*

and *bgl*, it is suggested that Bgl and CMCax work together to modulate cellulose in the late stages of culture of *Gluconacetobacter* (Kawano et al. 2008).

Production of nanofibrillated bacterial cellulose (NFBC) using *Gluconacetobacter*

Recently, nanofibrillated cellulose (NFC) with nano-order fiber width has been attracting attention as a new functional material. NFC has various features such as light weight, large surface area, and high mechanical strength, and is widely studied as a resin reinforcing material (filler). In general, NFC is prepared from pulp via a top-down process using various methods such as TEMPO oxidation method (Saito et al. 2006), grinder method (Abe et al. 2007; Abe and Yano 2009), underwater counter-collision method (Kose et al. 2011), and acid/enzyme hydrolysis method (Cranston and Gray 2006).

However, nanofibrillated bacterial cellulose (NFBC) can be prepared from a low-molecular-weight biomass, such as a sugar, via a bottom-up process by culturing a cellulose-producing bacterium in a medium supplemented with a dispersant, such as carboxymethyl cellulose (CMC), under aerobic and rotating culture conditions (Fig. 22). An extremely stable cellulose-producing bacterium [*G. intermedius* NEDO-01 (NITE P-1495)], suitable for NFBC production, has been identified and success is achieved in development of a method for large-scale production of NFBC using a jar fermenter (Kose et al. 2013). BC is generally produced as a gel-like membrane (pellicle), which is a three-dimensional network structure of cellulose nanofibers, by the static culture method. This method requires a lengthy culture period, and continuous culture is not possible, resulting in significantly low productivity. Furthermore, a pellicle having a strong three-dimensional network structure made of nanofibers has poor moldability, miscibility, and fluidity, and its application range as a material is limited. In contrast, production efficiency of NFBC can be improved by culturing a cellulose-producing bacterium using a jar fermenter under an optimized cultivation condition, such that cellulose is obtained as a homogeneously dispersed solution in one step. Furthermore, an amphiphilic

NFBC (HP-NFBC) can be easily obtained by changing the dispersant from CMC to hydroxypropylcellulose (HPC), an amphiphilic cellulose derivative (Tajima et al. 2017), and this is one of advantages for the bottom-up production of NFC. NFBC is superior in terms of dispersibility, fluidity, moldability, miscibility, and high aspect ratio (>500, Figs. 22 a and b). Moreover, this production methodology is a simple and versatile way to prepare new types of NFCs with a variety of useful functions. Currently, basic and applied researches are underway with the aim of using NFBC in various industrial materials (Tajima et al. 2017, 2020; Kono et al. 2020a, b; Akagi et al. 2021).

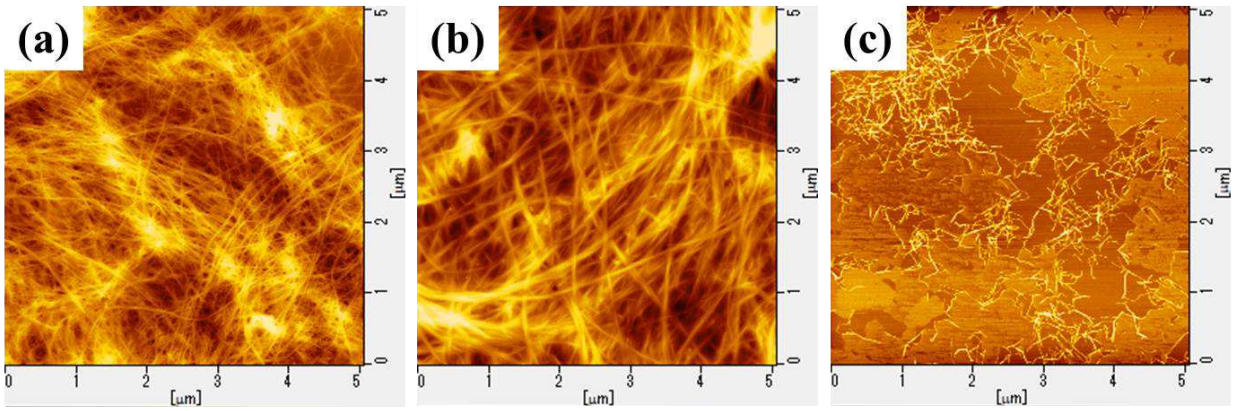

Fig. 22. Scanning probe microscope images of (a) CM-NFBC, (b) HP-NFBC, and (c) TEMPO-oxidized nanocellulose (TONC). CM- and HP-NFBCs were prepared by using carboxymethylcellulose (CMC) and hydroxypropylcellulose (HPC) as a dispersing agent, respectively. The partial of photographs have been reused from the reference (Akagi et al. 2021) with permission of Elsevier B.V.

Conclusions

Cellulose is produced mainly by plants, and is a major sink of atmospheric carbon dioxide. In addition to plants, a number of bacteria produce cellulose, many as part of the biofilm. The acetic acid bacteria, mainly *Gluconacetobacter*, are unique in producing large amounts of cellulose with many desirable properties. Strains of *G. xylinus* and *G. hansenii* are useful for understanding the basic mechanisms of cellulose biosynthesis, as well as large-scale production of bacterial cellulose. Even as new information is becoming available on the various proteins and their assembly into a cellulose-synthesizing complex in bacteria such as *E. coli*, limited understanding exists on the composition of the cellulose-synthesizing

machinery in *Gluconacetobacter* and how it is assembled. Currently, we are proceeding with structural and functional analyses of proteins associated with cellulose production in *Gluconacetobacter* and hope to look at assemblies of proteins in the near future. At the same time, research is continuing on the preparation of composites and copolymers by addition of various substances to the medium (Luo et al. 2008; Perotti et al. 2011; Kose et al. 2013; Orelma et al. 2014; Tajima et al. 2017; Gao et al. 2019) and by genetic engineering (Lee et al. 2001; Yadav et al. 2010; Fang et al. 2015; Florea et al. 2016; Teh et al. 2019) to produce cellulose-based environmentally-friendly materials using *Gluconacetobacter*.

Acknowledgements

This work was financially supported by a JSPS Grant-in-Aid for Scientific Research (A) (No. 19H00950, T.I.) and (B) (No. 19H02549, K.T.).

Ethics declarations

Conflict of interest
The authors declare that they have no conflict of interest.

Consent to participate
Not applicable.

Consent for publication
Not applicable.

Ethical approval
Not applicable.

Human/animal rights
This article does not contain any studies with human or animal subjects performed by any of the authors.

References

Abe K, Iwamoto S, Yano H (2007) Obtaining Cellulose Nanofibers with a Uniform Width of 15 nm from Wood. Biomacromolecules 8:3276–3278. https://doi.org/10.1021/bm700624p

Abe K, Yano H (2009) Comparison of the characteristics of cellulose microfibril aggregates of wood, rice straw and potato tuber. Cellulose 16:1017–1023. https://doi.org/10.1007/s10570-009-9334-9

Abidi W, Zouhir S, Caleechurn M, et al (2021) Architecture and regulation of an enterobacterial cellulose secretion system. Sci Adv 7:1–16. https://doi.org/10.1126/sciadv.abd8049

Acheson JF, Derewenda ZS, Zimmer J (2019) Architecture of the Cellulose Synthase Outer Membrane Channel and Its Association with the Periplasmic TPR Domain. Structure 27:1855-1861.e3. https://doi.org/10.1016/j.str.2019.09.008

Acheson JF, Ho R, Goularte NF, et al (2021) Molecular organization of the E. coli cellulose synthase macrocomplex. Nat Struct Mol Biol 28:310–318. https://doi.org/10.1038/s41594-021-00569-7

Akagi S, Ando H, Fujita K, et al (2021) Therapeutic efficacy of a paclitaxel-loaded nanofibrillated bacterial cellulose (PTX/NFBC) formulation in a peritoneally disseminated gastric cancer xenograft model. Int J Biol Macromol 174:494–501. https://doi.org/10.1016/j.ijbiomac.2021.01.201

Alzari PM, Souchon H, Dominguez R (1996) The crystal structure of endoglucanase CelA, a family 8 glycosyl hydrolase from Clostridium thermocellum. Structure 4:265–275. https://doi.org/10.1016/S0969-2126(96)00031-7

Benziman M, Haigler CH, Brown RM (1980) Cellulose biogenesis: Polymerization and crystallization are coupled processes in Acetobacter xylinum. Proc Natl Acad Sci U S A 77:6678–6682. https://doi.org/10.1073/pnas.77.11.6678

Brown AJ (1886) XLIII.—On an acetic ferment which forms cellulose. J Chem Soc, Trans 49:432–439. https://doi.org/10.1039/CT8864900432

Brown RM (1996) The Biosynthesis of Cellulose. J Macromol Sci Part A 33:1345–1373. https://doi.org/10.1080/10601329608014912

Brown RM, Willison JHM, Richardson CL (1976) Cellulose biosynthesis in Acetobacter xylinum: visualization of the site of synthesis and direct measurement of the in vivo process. Proc Natl Acad Sci U S A 73:4565–4569. https://doi.org/10.1073/pnas.73.12.4565

Castro C, Cleenwerck I, Trček J, et al (2013) Gluconacetobacter medellinensis sp. nov., cellulose- and non-cellulose-producing acetic acid bacteria isolated from vinegar. Int J Syst Evol Microbiol 63:1119–1125. https://doi.org/10.1099/ijs.0.043414-0

Chen HP, Brown RM (1996) Immunochemical studies of the cellulose synthase complex in Acetobacter xylinum. Cellulose 3:63–75. https://doi.org/10.1007/bf02228791

Cranston ED, Gray DG (2006) Morphological and optical characterization of polyelectrolyte multilayers incorporating nanocrystalline cellulose. Biomacromolecules 7:2522–2530. https://doi.org/10.1021/bm0602886

D'Andrea LD, Lynne R (2003) TPR proteins: the versatile helix. Trends Biochem Sci 28:655–662. https://doi.org/10.1016/j.tibs.2003.10.007

Du J, Vepachedu V, Cho SH, et al (2016) Structure of the cellulose synthase complex of Gluconacetobacter hansenii at 23.4 Å resolution. PLoS One 11:1–24. https://doi.org/10.1371/journal.pone.0155886

Fang J, Kawano S, Tajima K, Kondo T (2015) In Vivo Curdlan/Cellulose Bionanocomposite Synthesis by Genetically Modified Gluconacetobacter xylinus. Biomacromolecules 16:3154–3160. https://doi.org/10.1021/acs.biomac.5b01075

Florea M, Hagemann H, Santosa G, et al (2016) Engineering control of bacterial cellulose production using a genetic toolkit and a new celluloseproducing strain. Proc Natl Acad Sci U S A 113:E3431–E3440. https://doi.org/10.1073/pnas.1522985113

Fontana JD, De Souza AM, Fontana CK, et al (1990) Acetobacter cellulose pellicle as a temporary skin substitute. Appl Biochem Biotechnol 24–25:253–264. https://doi.org/10.1007/BF02920250

Fujiwara T, Komoda K, Sakurai N, et al (2013) The c-di-GMP recognition mechanism of the PilZ domain of bacterial cellulose synthase subunit A. Biochem Biophys Res Commun 431:802–807. https://doi.org/10.1016/j.bbrc.2012.12.103

Gao M, Li J, Bao Z, et al (2019) A natural in situ fabrication method of functional bacterial cellulose using a microorganism. Nat Commun 10:1–10. https://doi.org/10.1038/s41467-018-07879-3

Haigler CH, Brown RM, Benziman M (1980) Calcofluor white ST alters the in vivo assembly of cellulose microfibrils. Science (80-) 210:903–906. https://doi.org/10.1126/science.7434003

Haigler CH, Chanzy H (1988) Electron diffraction analysis of the altered cellulose synthesized by Acetobacter xylinum in the presence of fluorescent brightening agents and direct dyes. J Ultrastruct Res Mol Struct Res 98:299–311. https://doi.org/10.1016/S0889-1605(88)80922-4

Hon DNS (1994) Cellulose: a random walk along its historical path. Cellulose 1:1–25. https://doi.org/10.1007/BF00818796

Hu S-Q, Gao Y-G, Tajima K, et al (2010) Structure of bacterial cellulose synthase subunit D octamer with four inner passageways. Proc Natl Acad Sci 107:17957–17961. https://doi.org/10.1073/pnas.1000601107

Hyun Min K, Sung Hee S, Yu Ryang P, Yu Sam K (1998) Evidence That a β-1,4-Endoglucanase Secreted by Acetobacter xylinum Plays an Essential Role for the Formation of Cellulose Fiber. Biosci Biotechnol Biochem 62:2257–2259. https://doi.org/doi.org/10.1271/bbb.62.2257

Ifuku S, Nogi M, Abe K, et al (2007) Surface modification of bacterial cellulose nanofibers for property enhancement of optically transparent composites: Dependence on acetyl-group DS. Biomacromolecules 8:1973–1978. https://doi.org/10.1021/bm070113b

Iyer PR, Catchmark J, Brown NR, Tien M (2011) Biochemical localization of a protein involved in synthesis of Gluconacetobacter hansenii cellulose. Cellulose 18:739–747. https://doi.org/10.1007/s10570-011-9504-4

Kawano S, Tajima K, Kono H, et al (2002a) Effects of endogenous endo-β-1,4-glucanase on cellulose biosynthesis in Acetobacter xylinum ATCC23769. J Biosci Bioeng 94:275–281. https://doi.org/10.1016/S1389-1723(02)80162-1

925 Kawano S, Tajima K, Kono H, et al (2008) Regulation of endoglucanase gene (cmcax)
926 expression in Acetobacter xylinum. J Biosci Bioeng 106:88–94.
927 https://doi.org/10.1263/jbb.106.88

928 Kawano S, Tajima K, Uemori Y, et al (2002b) Cloning of cellulose synthesis related genes
929 from Acetobacter xylinum ATCC23769 and ATCC53582: Comparison of cellulose
930 synthetic ability between strains. DNA Res 9:149–156.
931 https://doi.org/10.1093/dnares/9.5.149

932 Kawano Y, Saotome T, Ochiai Y, et al (2011) Cellulose Accumulation and a Cellulose
933 Synthase Gene are Responsible for Cell Aggregation in the Cyanobacterium
934 Thermosynechococcus vulcanus RKN. Plant Cell Physiol 52:957–966.
935 https://doi.org/10.1093/pcp/pcr047

936 Kimura S, Chen HP, Saxena IM, et al (2001) Localization of c-di-GMP-Binding Protein with
937 the Linear Terminal Complexes of Acetobacter xylinum. J Bacteriol 183:5668–5674.
938 https://doi.org/10.1128/JB.183.19.5668-5674.2001

939 Klemm D, Schumann D, Udhardt U, Marsch S (2001) Bacterial synthesized cellulose -
940 Artificial blood vessels for microsurgery. Prog. Polym. Sci. 26:1561–1603

941 Knott BC, Crowley MF, Himmel ME, et al (2016) Simulations of cellulose translocation in
942 the bacterial cellulose synthase suggest a regulatory mechanism for the dimeric structure
943 of cellulose. Chem Sci 7:3108–3116. https://doi.org/10.1039/C5SC04558D

944 Kono H, Uno T, Tsujisaki H, et al (2020a) Nanofibrillated Bacterial Cellulose Surface
945 Modified with Methyltrimethoxysilane for Fiber-Reinforced Composites. ACS Appl
946 Nano Mater 3:8232–8241. https://doi.org/10.1021/acsanm.0c01670

947 Kono H, Uno T, Tsujisaki H, et al (2020b) Nanofibrillated Bacterial Cellulose Modified with
948 (3-Aminopropyl)trimethoxysilane under Aqueous Conditions: Applications to
949 Poly(methyl methacrylate) Fiber-Reinforced Nanocomposites. ACS Omega 5:29561–
950 29569. https://doi.org/10.1021/acsomega.0c04533

951 Kose R, Mitani I, Kasai W, Kondo T (2011) “Nanocellulose” as a single nanofiber prepared
952 from pellicle secreted by gluconacetobacter xylinus using aqueous counter collision.
953 Biomacromolecules 12:716–720. https://doi.org/10.1021/bm1013469

954 Kose R, Sunagawa N, Yoshida M, Tajima K (2013) One-step production of nanofibrillated
955 bacterial cellulose (NFBC) from waste glycerol using Gluconacetobacter intermedius
956 NEDO-01. Cellulose 20:2971–2979. https://doi.org/10.1007/s10570-013-0050-0

957 Koyama M, Helbert W, Imai T, et al (1997) Parallel-up structure evidences the molecular
958 directionality during biosynthesis of bacterial cellulose. Proc Natl Acad Sci U S A
959 94:9091–9095. https://doi.org/10.1073/pnas.94.17.9091

960 Kumagai A, Mizuno M, Kato N, et al (2011) Ultrafine cellulose fibers produced by asaia
961 bogorensis, an acetic acid bacterium. Biomacromolecules 12:2815–2821.
962 https://doi.org/10.1021/bm2005615

963 Lee JW, Deng F, Yeomans WG, et al (2001) Direct Incorporation of Glucosamine and N-
964 Acetylglucosamine into Exopolymers by Gluconacetobacter xylinus (=Acetobacter
965 xylinum) ATCC 10245: Production of Chitosan-Cellulose and Chitin-Cellulose
966 Exopolymers. Appl Environ Microbiol 67:3970–3975.
967 https://doi.org/10.1128/AEM.67.9.3970-3975.2001

968 Lin FC, Brown, Jr. RM (1989) Purification of cellulose synthase from Acetobacter xylinum.
969 In: Cellulose and Wood—Chemistry and Technology, C. Schuerc. John Wiley & Sons,
970 New York, pp 473–492

971 Lin FC, Brown RM, Drake RR, Haley BE (1990) Identification of the uridine 5'-
972 diphosphoglucose (UDP-Glc) binding subunit of cellulose synthase in Acetobacter
973 xylinum using the photoaffinity probe 5-azido-UDP-Glc. J Biol Chem 265:4782–4784.
974 https://doi.org/10.1016/s0021-9258(19)34039-6

975 Luo H, Xiong G, Huang Y, et al (2008) Preparation and characterization of a novel COL/BC
976 composite for potential tissue engineering scaffolds. Mater Chem Phys 110:193–196.
977 https://doi.org/10.1016/j.matchemphys.2008.01.040

978 Matthysse AG, Holmes K V., Gurlitz RHG (1981) Elaboration of cellulose fibrils by
979 Agrobacterium tumefaciens during attachment to carrot cells. J Bacteriol 145:583–595.
980 https://doi.org/10.1128/jb.145.1.583-595.1981

981 Mazur O, Zimmer J (2011) Apo- and cellopentaose-bound structures of the bacterial cellulose
982 synthase subunit BcsZ. J Biol Chem 286:17601–17606.
983 https://doi.org/10.1074/jbc.M111.227660

984 Mehta K, Pfeffer S, Brown RM (2015) Characterization of an acsD disruption mutant
985 provides additional evidence for the hierarchical cell-directed self-assembly of cellulose
986 in Gluconacetobacter xylinus. Cellulose 22:119–137. https://doi.org/10.1007/s10570-
987 014-0521-y

988 Morgan JLW, McNamara JT, Fischer M, et al (2016) Observing cellulose biosynthesis and
989 membrane translocation in crystallo. Nature 531:329–334.
990 https://doi.org/10.1038/nature16966

991 Morgan JLW, McNamara JT, Zimmer J (2014) Mechanism of activation of bacterial cellulose
992 synthase by cyclic di-GMP. Nat Struct Mol Biol 21:489–496.
993 https://doi.org/10.1038/nsmb.2803

994 Morgan JLW, Strumillo J, Zimmer J (2013) Crystallographic snapshot of cellulose synthesis
995 and membrane translocation. Nature 493:181–186. https://doi.org/10.1038/nature11744

996 Nakai T, Moriya A, Tonouchi N, et al (1998) Control of expression by the cellulose synthase
997 (bcsA) promoter region from Acetobacter xylinum BPR 2001. Gene 213:93–100.
998 https://doi.org/10.1016/S0378-1119(98)00191-7

999 Nakai T, Sugano Y, Shoda M, et al (2013) Formation of Highly Twisted Ribbons in a
1000 Carboxymethylcellulase Gene-Disrupted Strain of a Cellulose-Producing Bacterium. J
1001 Bacteriol 195:958–964. https://doi.org/10.1128/JB.01473-12

1002 Napoli C, Dazzo F, Hubbell D (1975) Production of cellulose microfibrils by Rhizobium.
1003 Appl Microbiol 30:123–131. https://doi.org/10.1128/aem.30.1.123-131.1975

1004 Nicolas WJ, Ghosal D, Tocheva EI, et al (2021) Structure of the bacterial cellulose ribbon and
1005 its assembly-guiding cytoskeleton by electron cryotomography. J Bacteriol 203:.
1006 https://doi.org/10.1128/JB.00371-20

1007 Nishi Y, Uryu M, Yamanaka S, et al (1990) The structure and mechanical properties of sheets
1008 prepared from bacterial cellulose - Part 2 Improvement of the mechanical properties of
1009 sheets and their applicability to diaphragms of electroacoustic transducers. J Mater Sci
1010 25:2997–3001. https://doi.org/10.1007/BF00584917

1011 Nobles DR, Romanovicz DK, Brown RM (2001) Cellulose in Cyanobacteria. Origin of
1012 Vascular Plant Cellulose Synthase? Plant Physiol 127:529–542.
1013 https://doi.org/10.1104/pp.010557

Nogi M, Abe K, Handa K, et al (2006a) Property enhancement of optically transparent bionanofiber composites by acetylation. Appl Phys Lett 89:233123. https://doi.org/10.1063/1.2403901

Nogi M, Ifuku S, Abe K, et al (2006b) Fiber-content dependency of the optical transparency and thermal expansion of bacterial nanofiber reinforced composites. Appl Phys Lett 88:133124. https://doi.org/10.1063/1.2191667

Nojima S, Fujishima A, Kato K, et al (2017) Crystal structure of the flexible tandem repeat domain of bacterial cellulose synthesis subunit C. Sci Rep 7:13018. https://doi.org/10.1038/s41598-017-12530-0

Omadjela O, Narahari A, Strumillo J, et al (2013) BcsA and BcsB form the catalytically active core of bacterial cellulose synthase sufficient for in vitro cellulose synthesis. Proc Natl Acad Sci 110:17856–17861. https://doi.org/10.1073/pnas.1314063110

Orelma H, Morales LO, Johansson L-S, et al (2014) Affibody conjugation onto bacterial cellulose tubes and bioseparation of human serum albumin. RSC Adv 4:51440–51450. https://doi.org/10.1039/C4RA08882D

Otsuka M, Fujiwara K, Sugai Y, et al (2004) Characterization of a water-insoluble polymer producing bacterium enterobacter sp. CJF-002 for MEOR. J Japan Pet Inst 47:282–292. https://doi.org/10.1627/jpi.47.282

Penttilä PA, Imai T, Capron M, et al (2018) Multimethod approach to understand the assembly of cellulose fibrils in the biosynthesis of bacterial cellulose. Cellulose 25:2771–2783. https://doi.org/10.1007/s10570-018-1755-x

Perotti GF, Barud HS, Messaddeq Y, et al (2011) Bacterial cellulose-laponite clay nanocomposites. Polymer (Guildf) 52:157–163. https://doi.org/10.1016/j.polymer.2010.10.062

Portela R, Leal CR, Almeida PL, Sobral RG (2019) Bacterial cellulose: a versatile biopolymer for wound dressing applications. Microb Biotechnol 12:586–610. https://doi.org/10.1111/1751-7915.13392

Römling U, Galperin MY (2015) Bacterial cellulose biosynthesis: Diversity of operons, subunits, products, and functions. Trends Microbiol. 23:545–557

Ross P, Mayer R, Benziman M (1991) Cellulose biosynthesis and function in bacteria. Microbiol. Rev. 55:35–58

Saito T, Nishiyama Y, Putaux JL, et al (2006) Homogeneous suspensions of individualized microfibrils from TEMPO-catalyzed oxidation of native cellulose. Biomacromolecules 7:1687–1691. https://doi.org/10.1021/bm060154s

Saxena IM, Brown RM, Fevre M, et al (1995) Multidomain architecture of beta-glycosyl transferases: implications for mechanism of action. J Bacteriol 177:1419–1424. https://doi.org/10.1128/JB.177.6.1419-1424.1995

Saxena IM, Kudlicka K, Okuda K, Brown RM (1994) Characterization of genes in the cellulose-synthesizing operon (acs operon) of Acetobacter xylinum: Implications for cellulose crystallization. J Bacteriol 176:5735–5752. https://doi.org/10.1128/jb.176.18.5735-5752.1994

Saxena IM, Lin FC, Brown RM (1990) Cloning and sequencing of the cellulose synthase catalytic subunit gene of Acetobacter xylinum. Plant Mol Biol 15:673–683. https://doi.org/10.1007/BF00016118

Schmidt A, Gonzalez A, Morris RJ, et al (2002) Advantages of high-resolution phasing: MAD to atomic resolution. Acta Crystallogr Sect D Biol Crystallogr 58:1433–1441. https://doi.org/10.1107/S0907444902011368

Shah J, Malcolm Brown R (2005) Towards electronic paper displays made from microbial cellulose. Appl Microbiol Biotechnol 66:352–355. https://doi.org/10.1007/s00253-004-1756-6

Standal R, Iversen TG, Coucheron DH, et al (1994) A new gene required for cellulose production and a gene encoding cellulolytic activity in Acetobacter xylinum are colocalized with the bcs operon. J. Bacteriol. 176:665–672

Sun S, Imai T, Sugiyama J, Kimura S (2017) CesA protein is included in the terminal complex of Acetobacter. Cellulose 24:2017–2027. https://doi.org/10.1007/s10570-017-1237-6

Sunagawa N, Fujiwara T, Yoda T, et al (2013) Cellulose complementing factor (Ccp) is a new member of the cellulose synthase complex (terminal complex) in Acetobacter xylinum. J Biosci Bioeng 115:607–612. https://doi.org/10.1016/j.jbiosc.2012.12.021

Sunagawa N, Tajima K, Hosoda M, et al (2012) Cellulose production by Enterobacter sp. CJF-002 and identification of genes for cellulose biosynthesis. Cellulose 19:1989–2001. https://doi.org/10.1007/s10570-012-9777-2

Tahara N, Tonouchi N, Yano H, Yoshinaga F (1998a) Purification and characterization of exo-1,4-β-glucosidase from Acetobacter xylinum BPR2001. J Ferment Bioeng 85:589–594. https://doi.org/10.1016/S0922-338X(98)80010-X

Tahara N, Yano H, Yoshinaga F (1998b) Subsite structure of exo-1,4-β-glucosidase from Acetobacter xylinum BPR2001. J Ferment Bioeng 85:595–597. https://doi.org/10.1016/S0922-338X(98)80011-1

Tajima K, Kusumoto R, Kose R, et al (2017) One-Step Production of Amphiphilic Nanofibrillated Cellulose Using a Cellulose-Producing Bacterium. Biomacromolecules 18:3432–3438. https://doi.org/10.1021/acs.biomac.7b01100

Tajima K, Nakajima K, Yamashita H, et al (2001) Cloning and sequencing of the beta-glucosidase gene from Acetobacter xylinum ATCC 23769. DNA Res 8:263–269. https://doi.org/10.1093/dnares/8.6.263

Tajima K, Tahara K, Ohba J, et al (2020) Detailed Structural Analyses of Nanofibrillated Bacterial Cellulose and Its Application as Binder Material for a Display Device. Biomacromolecules 21:581–588. https://doi.org/10.1021/acs.biomac.9b01328

Teh MY, Ooi KH, Danny Teo SX, et al (2019) An Expanded Synthetic Biology Toolkit for Gene Expression Control in Acetobacteraceae. ACS Synth Biol 8:708–723. https://doi.org/10.1021/acssynbio.8b00168

Thongsomboon W, Serra DO, Possling A, et al (2018) Phosphoethanolamine cellulose: A naturally produced chemically modified cellulose. Science (80-) 359:334–338. https://doi.org/10.1126/science.aao4096

Tonouchi N, Tahara N, Kojima Y, et al (1997) A Beta-Glucosidase Gene Downstream of the Cellulose Synthase Operon in Cellulose-producing Acetobacter. Biosci Biotechnol Biochem 61:1789–1790. https://doi.org/10.1271/bbb.61.1789

Tonouchi N, Tahara N, Tsuchida T, et al (1995) Addition of a Small Amount of an Endoglucanase Enhances Cellulose Production by Acetobacter xylinum. Biosci Biotechnol Biochem 59:805–808. https://doi.org/10.1271/bbb.59.805

Umeda Y, Hirano A, Ishibashi M, et al (1999) Cloning of cellulose synthase genes from Acetobacter xylinum JCM 7664: Implication of a novel set of cellulose synthase genes. DNA Res 6:109–115. https://doi.org/10.1093/dnares/6.2.109

Uto T, Ikeda Y, Sunagawa N, et al (2021) Molecular Dynamics Simulation of Cellulose Synthase Subunit D Octamer with Cellulose Chains from Acetic Acid Bacteria: Insight into Dynamic Behaviors and Thermodynamics on Substrate Recognition. J Chem Theory Comput 17:488–496. https://doi.org/10.1021/acs.jctc.0c01027

Wang X, Kong D, Zhang Y, et al (2016) All-biomaterial supercapacitor derived from bacterial cellulose. Nanoscale 8:9146–9150. https://doi.org/10.1039/C6NR01485B

Whitney JC, Howell PL (2013) Synthase-dependent exopolysaccharide secretion in Gram-negative bacteria. Trends Microbiol 21:63–72. https://doi.org/10.1016/j.tim.2012.10.001

Wong HC, Fear AL, Calhoon RD, et al (1990) Genetic organization of the cellulose synthase operon in Acetobacter xylinum. Proc Natl Acad Sci U S A 87:8130–8134. https://doi.org/10.1073/pnas.87.20.8130

Yadav V, Paniliatis BJ, Shi H, et al (2010) Novel in vivo-degradable cellulose-chitin copolymer from metabolically engineered gluconacetobacter xylinus. Appl Environ Microbiol 76:6257–6265. https://doi.org/10.1128/AEM.00698-10

Yamada Y, Yukphan P (2008) Genera and species in acetic acid bacteria. Int J Food Microbiol 125:15–24. https://doi.org/10.1016/j.ijfoodmicro.2007.11.077

Yamada Y, Yukphan P, Vu HTL, et al (2012) Description of Komagataeibacter gen. nov., with proposals of new combinations (Acetobacteraceae). J Gen Appl Microbiol 58:397–404. https://doi.org/10.2323/jgam.58.397

Yano H, Sugiyama J, Nakagaito AN, et al (2005) Optically Transparent Composites Reinforced with Networks of Bacterial Nanofibers. Adv Mater 17:153–155. https://doi.org/10.1002/adma.200400597

Yasutake Y, Kawano S, Tajima K, et al (2006) Structural characterization of the Acetobacter xylinum endo-β-1,4-glucanase CMCax required for cellulose biosynthesis. Proteins Struct Funct Bioinforma 64:1069–1077. https://doi.org/10.1002/prot.21052

Zaar K (1979) The Gram-negative bacterium Acetobacter xylinum assembles a cellulose ribbon composed of a number of microfibrils in the longitudinal axis of its envelope . The zone of ribbon assembly was investigated by freeze-etch electron microscopy . Freeze-etching r. J Cell Biol 80:773–777

Zang S, Zhang R, Chen H, et al (2015) Investigation on artificial blood vessels prepared from bacterial cellulose. Mater Sci Eng C 46:111–117. https://doi.org/10.1016/j.msec.2014.10.023

Figure Legends

Fig. 1 Diversity of the bacterial cellulose synthase (*bcs*) operons. The displayed operons are from *Komagataeibacter xylinus* E25 (I_a), *Dickeya dadantii* Ech703 (I_b), *Burkholderia phymatum* STM815 (I_c), *Salmonella enterica* serovar Typhimurium (II_a), *Pseudomonas putida* KT2440 (II_b), *Burkholderia mallei* ATCC 23344 (II_c), *Chromobacterium violaceum* ATCC 12472 (II_d), *Agrobacterium fabrum* C58 (III_a), *Methylobacterium extorquens* PA1 (III_b), *Azospirillum lipoferum* 4B (III_c), *Acidiphilium cryptum* JF-5 (III_d), *Nostoc punctiforme* PCC 73102 (IV_a), and *Nostoc* sp. PCC 7120 (IV_b). This figure is from Römling and Galperin 2015, and is used with permission of Elsevier.

Fig. 2 (a) TEM image of *G. xylinus* cell producing a cellulose ribbon. (b) Nata de coco. (c) scanning electron microscope (SEM) image of lyophilized Nata de coco showing cellulose fibrils.

Fig. 3 Generalized model of ribbon assembly in *Gluconacetobacter*. The boxes show possible packing arrangements of the 1.5nm tactoidal aggregates. This figure is reproduced from Ross et al. 1991, and is used with permission of American Society for Microbiology.

Fig. 4 Labeling of *Gluconacetobacter xylinus* ATCC 53524 with colloidal gold-bound antibody against BcsB. A linear pattern of labeling is observed despite non-specific labeling. This figure is from Sun et al. 2017, and is used with permission of Springer Nature.

Fig. 5 Fluorescence micrographs of *Gluconacetobacter* cells following immunolabeling with antibodies against BcsA (= CesA) and BcsD (= CesD). The phase-contrast s and epi-fluorescence images are merged. A Cells from three different strains (ATCC 53524, ATCC 53264, and JCM 9730) were labeled using an identical protocol. Insets show images at higher magnification. B Control experiments using strain ATCC 53524. Combination of primary and secondary antibodies used is as indicated. Almost no labeling was found. This figure is from Sun et al. 2017, and is used with permission of Springer Nature.

Fig. 6 Labeling of the *bcsD*-knockout mutant (DBCD) of *Gluconacetobacter* expressing native EGFP (pTIEK) or the BcsD-EGFP-fusion protein (pTIDEK). This figure is from Sunagawa et al. 2013, and is used with permission of Elsevier B.V.

Fig. 7 Labeling of *Gluconacetobacter* with enhanced green fluorescent protein (EGFP) [Cel-1(pTIE)] or Ccp-EGFP fusion protein [Cel-1(pTI21E), Cel-1(pTI22E), and Cel-1(pTI23E)]. This figure is from Sunagawa et al. 2013, and is used with permission of Elsevier B.V.

Fig. 8 Updated cell-directed hierarchical model. Top (left) and side (right) views of a *G. hansenii* cell showing the different aggregation steps leading to a cellulose sheet, how microfibrils contribute to sheet width, and the role of the cortical belt. In this model, clusters of 11 extrusion pores are depicted (green circles); the real numbers and distribution are unknown. Each extrusion pore is presented as comprising 5 BcsC subunits (red circles); the actual number is not known. On the right is a magnified view of the line of 11 extrusion pores, each hypothesized to extrude an aggregate of multiple elementary fibrils (yellow dashed lines). All aggregates then

coalesce to form a microfibril of increasing thickness as it incorporates an increasing number of elementary fibril aggregates. These microfibrils then stack together, contributing to the width of the cellulose sheet (Nicolas et al. 2021: W. J. Nicolas, D. Ghosal, E. I. Tocheva, E. M. Meyerowitz, G. J. Jensen, *J. Bacteriol.* **203**, e00371-20 DOI: 10.1128/JB.00371-20). Published by The American Society for Microbiology.

Fig. 9 Model structure of the BcsA-BcsB complex from *G. hansenii* ATCC 23769 (red) predicted by Phyre2 (http://www.sbg.bio.ic.ac.uk/~phyre2/html/page.cgi?id=index) using BcsA-BcsB complex (PDB: 5EJ1, blue) from *R. sphaeroides* as a template.

Fig. 10 Modeling of BcsA from *G. hansenii* ATCC 23769 by Phyre2 (http://www.sbg.bio.ic.ac.uk/~phyre2/html/page.cgi?id=index) using BcsA from *R. sphaeriides* as a template.

Fig. 11 3D reconstruction of negatively stained BcsA-BcsB complex (= AcsAB) from *G. hansenii* ATCC 23769 at 23.4 Å. (a) Three side views of 3D reconstructed model of BcsA-BcsB complex. The volume of BcsA is composed of membrane embedded TM region and a large cytosolic region. The active site responsible for substrate binding and PilZ domain required for activator c-di-GMP binding are mapped in the cytosolic region. The density of BcsB sits on the top of BcsA. The cytoplasmic membrane boundaries are represented by black lines. (b) The BcsA-BcsB EM density map was docked with crystal structure of BcsA-BcsB (PDB: 4HG6). BcsA and BcsB are shown in orchid and cyan ribbon representatives, respectively. The translocating glucan co-crystallized with BcsA-BcsB is indicated in cyan sphere (Du et al. 2016: J. Du, V. Vepachedu, S. Hyun Cho, M. Kumar, and B. T. Nixon *PLoS ONE* **11**, e0155886 DOI: 10.1371/journal.pone.0155886).

Fig. 12 The hypothesized processive cycle of the bacterial cellulose synthase (Knott et al. 2016: B. C. Knott, M. F. Crowley, M. E. Himmel, J. Zimmer and G. T. Beckham, *Chem. Sci.*, 2016, **7**, 3108 DOI: 10.1039/C5SC04558D). Published by The Royal Society of Chemistry.

Fig. 13 Structures of PilZ domain of BcsAs from *G. hansenii* ATCC 23769 (PDB: 4I86, red) and *R. sphaeroides* (PDB: 4P00, blue).

Fig. 14 Model structures of BcsC from *G. hansenii* ATCC 23769 (red) obtained using Phre2 and BcsC (PDB: 6TZK, blue) from *E. coli* as the template.

Fig. 15 The structure of BcsC-TPR(N6) from *Enterobacter* sp. CJF-002 (A) BcsC-TPR(N6) is composed of six TPR motifs (colored blue, light blue, green, yellow, orange, and red) and two unpaired α-helices (gray). (B) Schematic diagram of the secondary structure of BcsC-TPR(N6). The boxes indicate α-helices and the lines indicate turns. The color scheme is the same as in (A). (Nojima et al. 2017: S. Nojima, A. Fujishima, K. Kato, K. Ouchi, N. Shimizu, K. Yonezawa, K. Tajima, and M. Yao. *Sci Rep* 2017, **7**, 13018 DOI: 10.1038/s41598-017-12530-0). Published by Springer Nature.

Fig. 16 Crystal structure of BcsD (= CeSD) from *G. hansenii* ATCC 23769. (A) Ribbon representation of the dimeric structure of BcsD. The two monomers are shown in blue and red, respectively. The helices and sheets are labeled, where the prime refers to the second monomer. (B) Overall structure of the BcsD octamer. The octamer structure is viewed along the 4-fold axis (top view) and the dyad axis (side view), with each monomer (A–H) shown in a different color. The N and C termini of all copies that are positioned in the center and outside of the cylinder are indicated by

the circled N and C (same as in A), respectively. (C) A schematic diagram of the octamer assembly based on the side view in B. The octamer is represented by a cylinder, and monomers (A, C, E, G) and (B, D, F, H) are distributed in the top and bottom layers, respectively. The colors of each molecule correspond with those in B. The dimer–dimer interfaces are depicted with sloping rectangles, and indicated by arrows. A and B were prepared using the program PyMOL (DeLano Scientific LLC, http://pymol.sourceforge.net/) (Hu et al. 2010: S.-Q. Hu, Y.-G. Gao, K. Tajima, N. Sunagawa, Y. Zhou, S. Kawano, T. Fujiwara, T. Yoda, D. Shimura, Y. Satoh, M. Munekata, I. Tanaka, and M. Yao 2010, PNAS, 107, 17957–17961 DOI: 10.1073/pnas.1000601107). Published by the National Academy of Sciences.

Fig. 17 Effects of deletions and mutations in *bcsD* (= *cesD*) on cellulose production. BcsDs (= CeSDs) with different lengths of N-terminal deletions were expressed in the DBCD strain of *G. hansenii* ATCC 23769. (A) The relative yield of cellulose produced by wild-type (WT), *bcsD* deletion mutant with a control vector (DBCD), *bcsD* deletion mutant with full-length Bcs*D* (DBCD+D), *bcsD* deletion mutant with BcsD in which four N-terminal residues are deleted (DBCD+DΔN4), *bcsD* deletion mutant with BcsD in which five N-terminal residues are deleted (DBCD+DΔN5), and *bcsD* deletion mutant with BcsD in which six N-terminal residues are deleted (DBCD+DΔN6).(B) Molecular surface of octamers of wild-type BcsD (WT; the three N-terminal residues are disordered), BcsD with deletion of the five N-terminal residues (DΔN5) (), and BcsD with deletion of the six N-terminal residues (DΔN6). (Hu et al. 2010: S.-Q. Hu, Y.-G. Gao, K. Tajima, N. Sunagawa, Y. Zhou, S. Kawano, T. Fujiwara, T. Yoda, D. Shimura, Y. Satoh, M. Munekata, I. Tanaka, and M. Yao 2010, PNAS, 107, 17957–17961 DOI: 10.1073/pnas.1000601107). Published by the National Academy of Sciences).

Fig. 18 A model of the BcsD(= CeSD)-G12 complex. a) Shape of a cellulose chain in the sugar chain pathway between BcsD dimers. b) Three-dimensional structural change of the pyranose ring of the glucose residues at the bend. $^4C_1$ corresponds to the original pyranose ring chair structure. This figure is from Uto et al. 2020and is used with permission of the American Chemical Society.

Fig. 19 Confirmation of interaction between Ccp and BcsD (= CeSD) by a pulldown assay. (a) SDS-PAGE gel; (b) Western blot using an anti-Ccp antibody; (c) Western blot using an anti-EGFP antibody; (d) SDS-PAGE gel. For (a), (b), and (c): M: marker; C: JM109(pTIE); lane 1: JM109(pSHD/pTIE); lane 2: JM109(pSHD/pTI23E); lane 3: JM109(pSTV28/pTI23E); 4: JM109(pSTV28/pTIE). For (d): M: marker; lane 1: debris; lane 2: crude lysate; lane 3: flow through; lane 4: elution fraction 1; lane 5: elution fraction 2. This figure is from Sunagawa et al. 2013, and is used with permission of Elsevier B.V.

Fig. 20 Molecular surface potential representation of CtCelA (PDB code, 1kwf) and CMCax. The model of substrate in the structure 1kwf is also shown in the cleft of CMCax. The electrostatic surface potentials were generated using PyMol (DeLano Scientific LLC, http://pymol.sourceforge.net/) in absolute mode. Areas colored in white, red, and blue denote neutral, negative and positive potential, respectively. This figure is used with permission from John Wiley & Sons, Inc.

Fig. 21 Model structure of β-glucosidase (Bgl) from *G. hansenii* ATCC 23769 predicted by Phyre2 using Bgl (PDB: 3AC0) from *Kluyveromyces marxianus* as a template.

Fig. 22 Scanning probe microscope images of (a) CM-NFBC, (b) HP-NFBC, and (c) TEMPO-oxidized nanocellulose (TONC). CM- and HP-NFBCs were prepared by using carboxymethylcellulose (CMC) and hydroxypropylcellulose (HPC) as a dispersing agent, respectively. The partial of photographs have been reused from the reference (Akagi et al. 2021) with permission of Elsevier B.V.

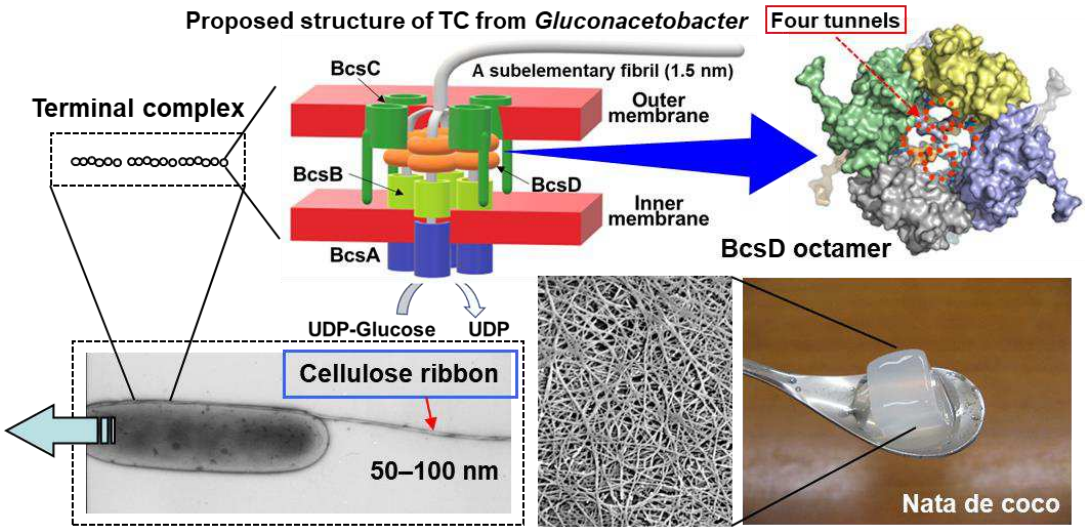
Proposed structure of TC from *Gluconacetobacter*
Four tunnels
Terminal complex
BcsC
A subelementary fibril (1.5 nm)
Outer membrane
BcsB
BcsD
Inner membrane
BcsA
BcsD octamer
UDP-Glucose
UDP
Cellulose ribbon
50–100 nm
Nata de coco